Hindawi
International Journal of Aerospace Engineering
Volume 2021, Article ID 6669380, 18 pages
https://doi.org/10.1155/2021/6669380

Research Article

Noncertainty Equivalent Adaptive Backstepping Control for Advanced Fighter Subject to Unsteady Effects and Input Constraints

Chijun Zhou,[1] Changxin Luo ,[1] Jikun Ye,[1] Jihong Zhu,[2] and Humin Lei[1]

[1]*Air and Missile Defense College, Air Force Engineering University, Xi'an 710051, China*
[2]*Department of Precision Instruments, Tsinghua University, Beijing 100084, China*

Correspondence should be addressed to Changxin Luo; 1710794652@qq.com

Received 4 October 2020; Revised 15 December 2020; Accepted 4 January 2021; Published 7 April 2021

Academic Editor: Kenneth M. Sobel

Copyright © 2021 Chijun Zhou et al. This is an open access article distributed under the Creative Commons Attribution License, which permits unrestricted use, distribution, and reproduction in any medium, provided the original work is properly cited.

This paper presents a noncertainty equivalent adaptive backstepping control scheme for advanced fighter attitude tracking, in which unsteady effects, parameter uncertainties, and input constraints are all considered which increase the design difficulty to a large extent. Based on unsteady attitude dynamics and the noncertainty equivalent principle, a new observer is first developed to reconstruct the immeasurable and time-varying unsteady states. Afterwards, the unsteady aerodynamics is compensated in the backstepping controller where the command filter is introduced to impose physical constraints on actuators. In order to further enhance the robustness, the noncertainty equivalent adaptive approach is again used to estimate the uncertain constant parameters. Moreover, stability of the closed-loop system that includes the state observer, parameter estimator, and backstepping controller is proven by the Lyapunov theorem in a unified architecture. Finally, simulation results show that performance of the deterministic control system can be captured when attractive manifolds are achieved. The effectiveness and robustness of the proposed control scheme are verified by the Herbst maneuver.

1. Introduction

Flight envelopes are substantially extended by the fourth generation fighter which directly leads to urgent demands for higher performance control laws. Since full envelope dynamics of aircraft is nonlinear and involves wide variations in aerodynamic parameters, traditional linear control methods are incapable of addressing such challenges [1]. Therefore, to ensure adequate stability and tracking performance in extreme flight regimes, a number of nonlinear control techniques have been extensively investigated, such as dynamic inversion [2, 3], fuzzy logic [4], neural network [5], backstepping [6], and sliding mode control [7]. In particular, Lyapunov-based backstepping control is among the most widely studied of these methods. Due to the cascaded structure of aircraft dynamics, many efforts have been made to develop a flight control system via the combination of backstepping theory and other control technologies, such as disturbance observer [8], radial basis function neural network [9], and adaptive control method [10, 11].

Generally, adaptive backstepping provides a systematic approach to solve the tracking or regulation problems of uncertain nonlinear systems. However, it must be noted that the adaptive backstepping control methods mentioned above have not considered input constraints which cannot be ignored in practice due to the existence of physical limits on actuators [12]. When aircraft maneuvers at a high angle of attack (AOA), drastic decreases of control authority often causes aerodynamic surface saturation which may severely degrade control performance by giving undesirable inaccuracy or leading to instability [13]. In some applications, this problem is crucial, especially in combination with online approximation-based control, which tends to be aggressive in seeking desired tracking performance [14]. For the purpose of circumventing this dilemma, it is necessary to take the input constraints into account at the level of the control design. In constraint adaptive control, the key issue is how

to analyze the constraint effects on a closed-loop system. Toward this end, an auxiliary system of which states are used for feedback control is proposed in [15, 16]. Recently, it was incorporated into backstepping architecture to solve trajectory tracking problems for reentry vehicles and air-breathing hypersonic vehicles in the presence of actuator constraints [17–19]. In addition, the command filter adaptive backstepping control proposed in [14, 20] is also a wise choice to tackle input constraints, in which the command filter is used to calculate the derivatives of virtual controls and impose constraints on states and inputs. This control scheme is presented for the F-16/MATV fighter in [21], where tracking errors in adaptive laws are replaced by compensated errors; hence, the adaption process can be isolated, i.e., not affected by saturation of virtual controls or actuators.

Besides model uncertainties and input constraints, unsteady effects are also potential issues that should be considered for an advanced fighter. Unsteady aerodynamic states are immeasurable in practice and may change rapidly during maneuvers which pose additional challenges for control [22]. Due to the difficulties in unsteady aerodynamic modelling, unsteady effects are usually treated as a part of model uncertainties which increase robust requirements for control system design. Based on an unsteady aerodynamic model, an alternative way is to estimate the unsteady effects via state observation and then make compensation in the controller design. Generally, it is not difficult to merely handle state observation, but the complexity increases drastically when uncertainties and input constraints are all considered. In recent years, a novel approach for stabilization and adaptive control of uncertain nonlinear systems based on immersion and invariance (I&I) methodology has been proposed in [23] and then further developed in [24, 25]. This method gives a noncertainty equivalent adaptive (NCEA) law which is different from the traditional certainty equivalent adaptive (CEA) method. The main feature of this approach lies in the construction of an estimator, which is a sum of a partial estimate generated by an update law and a judiciously chosen nonlinear function. The essential idea is to create a manifold in the extended space of states and parameters to which trajectories are attracted. As the trajectory evolves on this manifold, the closed-loop system captures the behavior of a deterministic system [26]. Due to the advantages in prescribing estimate error dynamics and separately synthesizing controller and estimator, this method shows great potential for uncertain nonlinear systems with complex structures. However, it relies on solving a partial differential equation (PDE), which is difficult for multivariable systems [27]. To overcome this difficulty, auxiliary state filter and regressor matrix filter are introduced [28–30]. Recently, its applications to the control of missiles, quad-rotor UAVs, and satellites are studied successively [26, 31, 32]. Apart from flight control, the I&I approach is also applied in aeroelastic control [33] and mechatronic systems [34].

In this research, a novel adaptive backstepping control scheme based on noncertainty equivalent principle is proposed for advanced fighter attitude tracking. Compared with our preceding study in [35], the prior hypothesis about the upper bounds of the uncertainties is removed, and the input constraints are dealt with in a simpler way. Moreover, the coupling relationship of the observer and estimator is considered fully in the closed-loop design. Therefore, the main contributions of this paper can be summarized as follows:

(1) The I&I method is used to estimate not only immeasurable states but also unknown parameters; it is further modified with different forms in these two situations and is closely associated with the characteristics of an advanced fighter

(2) The mutual effects of unsteady states and parameter uncertainties make the closed-loop control design complex. The observer and estimator are coupled together, but the coupling effects can be weakened by selecting appropriate parameters; in other words, the observer and estimator can be designed to satisfy the spectrum separation principle

(3) The proposed control scheme involves a state observer, a constraint backstepping controller, and two parameter estimators which are designed separately, but the stability of the closed-loop system is proven in a unified architecture

The rest of this paper is organized as follows. In the next section, unsteady attitude dynamics is modeled. The third section details the derivation of the state observer. In the fourth section, the constraint adaptive backstepping control design and stability analysis are presented. Simulations and conclusions are given in fifth and sixth sections, respectively.

2. Unsteady Attitude Dynamics

The model adopted in this research is a certain advanced fighter which is developed to investigate the flight dynamics during high AOA maneuvers. The fighter attitude dynamics is formulated as

$$\begin{bmatrix} \dot{V}_t \\ \dot{\beta} \\ \dot{\alpha} \end{bmatrix} = \begin{bmatrix} 0 \\ -r_s \\ q_s - p_s \tan\beta \end{bmatrix} + \Lambda T_{w/b} \begin{bmatrix} \bar{X} + T_x + G_x \\ \bar{Y} + T_y + G_y \\ \bar{Z} + T_z + G_z \end{bmatrix},$$

$$\begin{bmatrix} \dot{p}_s \\ \dot{q}_s \\ \dot{r}_s \end{bmatrix} = \begin{bmatrix} r_s\dot{\alpha} \\ 0 \\ -p_s\dot{\alpha} \end{bmatrix} + T_{s/b} \begin{bmatrix} (c_1 r + c_2 p)q + c_3(L_A + L_T) + c_4(N_A + N_T) \\ c_5 pr - c_6(p^2 - r^2) + c_7(M_A + M_T) \\ (c_8 p - c_2 r)q + c_4(L_A + L_T) + c_9(N_A + N_T) \end{bmatrix}, \tag{1}$$

where $\Lambda = \mathrm{diag}\,[1/m, 1/(mV_t), 1/(mV_t \cos\beta)]$, $T_{w/b}$, $T_{s/b}$ represent the rotation matrices from body axis system to wind axis system and stability axis system, respectively, and c_i, $i = 1, 2, \cdots, 9$ are inertia parameters defined in [21].

The fighter is equipped with two kinds of actuators, i.e., the aerodynamic surfaces and thrust vector engines, all of which are modeled as a first-order filter with limits in magnitude and rate (see Table 1). The sketch of the thrust vector control is depicted in Figure 1.

Table 1: Physical constraints on actuators.

Control inputs	Bandwidth (rad/s)	Magnitude limit (°)	Rate limit (°/s)
δ_a	20	[-20, 20]	[-80, 80]
δ_e	20	[-20, 20]	[-100, 100]
δ_r	20	[-25, 25]	[-120, 120]
$\delta_{yl}, \delta_{yr}, \delta_{zl}, \delta_{zr}$	15	[-20, 20]	[-50, 50]

The thrust forces and moments are defined as

$$\begin{bmatrix} T_x \\ T_y \\ T_z \end{bmatrix} = \begin{bmatrix} T\cos\delta_{yl}\cos\delta_{zl} + T\cos\delta_{yr}\cos\delta_{zr} \\ T\sin\delta_{yl} + T\sin\delta_{yr} \\ -T\cos\delta_{yl}\sin\delta_{zl} - T\cos\delta_{yr}\sin\delta_{zr} \end{bmatrix},$$

$$\begin{bmatrix} L_T \\ M_T \\ N_T \end{bmatrix} = Tx_T \begin{bmatrix} 0 \\ -\cos\delta_{yl}\sin\delta_{zl} - \cos\delta_{yr}\sin\delta_{zr} \\ -\sin\delta_{yl} - \sin\delta_{yr} \end{bmatrix} + \frac{Ty_T}{2} \begin{bmatrix} \cos\delta_{yl}\sin\delta_{zl} - \cos\delta_{yr}\sin\delta_{zr} \\ 0 \\ \cos\delta_{yl}\cos\delta_{zl} - \cos\delta_{yr}\cos\delta_{zr} \end{bmatrix}. \quad (2)$$

The aerodynamic model is extracted from wind tunnel tests which are conducted on sufficiently close points to capture the nonlinear behavior of the aerodynamics. Based on linear superposition principle, the aerodynamic forces and moments are expressed by

$$\begin{cases} \bar{X} = QS\bar{C}_X, \\ \bar{Y} = QS\left(\bar{C}_Y + C_{Y\delta_a}\delta_a + C_{Y\delta_r}\delta_r + \eta_Y\right), \\ \bar{Z} = QS\left(\bar{C}_Z + C_{Z\delta_e}\delta_e + \eta_Z\right), \\ L_A = QSb\left(\bar{C}_l + C_{l\delta_a}\delta_a + C_{l\delta_r}\delta_r + \eta_l\right), \\ M_A = QS\bar{c}\left(\bar{C}_m + C_{m\delta_e}\delta_e + \eta_m\right), \\ N_A = QSb\left(\bar{C}_n + C_{n\delta_a}\delta_a + C_{n\delta_r}\delta_r + \eta_n\right), \end{cases} \quad (3)$$

where $\eta_Y, \eta_Z, \eta_l, \eta_m, \eta_n$ represent the unsteady states, and the expressions of $\bar{C}_i, i = X, Y, Z, l, m, n$, are given in [36]. Unsteady effects on the axial force are neglected since the axial force measured in the test is small in contrast to other aerodynamic forces [36].

Usually, the quasisteady model in which unsteady states are equal to zero can be employed to describe the aerodynamics in normal flight condition. However, owing to notable effects caused by separated and vortical flow, it becomes inadequate to describe the aircraft dynamics at high AOA.

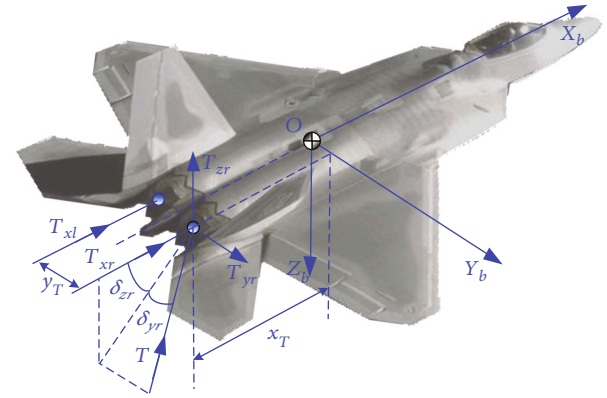

Figure 1: Sketch of the thrust vector control and its relevant variables.

Thus, unsteady aerodynamics are introduced and modeled in the following form [37, 38]:

$$\dot{\eta} = h(x) - \mathbf{B}(\sigma)\eta, \quad (4)$$

where $\eta = [\eta_Y, \eta_Z, \eta_l, \eta_m, \eta_n]^T$ is the immeasurable unsteady state; $h(x) = [a_Y\dot{\beta}, a_Z\dot{\alpha}, a_l\dot{\beta}, a_m\dot{\alpha}, a_n\dot{\beta}]^T$; $\mathbf{B}(\sigma) = \text{diag}\,[b_Y, b_Z, b_l, b_m, b_n]$, $b_i > 0$; and $a_i, b_i, i = Y, Z, l, m, n$, are fitting polynomials given in [36]. Note that the unsteady effects will converge to zero exponentially as the maneuver ends since (4) is stable.

3. Unsteady State Observation

The main objective of this section is to develop a nonlinear state observer which precisely reconstructs the unsteady states in the presence of parameter uncertainties. To this end, the attitude dynamics used for state observation and control design are rewritten as

$$\begin{cases} \dot{\sigma} = \mathbf{f}_1(\mathbf{x}) + \mathbf{W}_1(\mathbf{x})\eta + \mathbf{G}_1\bar{\omega} + \mathbf{D}_1(\sigma)\theta_1, \\ \dot{\omega} = \mathbf{f}_2(\mathbf{x}) + \mathbf{W}_2(\mathbf{x})\eta + \mathbf{G}_2(\sigma)u + \mathbf{D}_2(\sigma)\theta_2, \\ \dot{\eta} = h(x) - \mathbf{B}(\sigma)\eta, \end{cases} \quad (5)$$

where $\sigma = [\alpha, \beta]^T$ is the incidence angle, $\omega = [p_s, q_s, r_s]^T$ represents the stability axis angular rate, $x = [\sigma^T, \omega^T]^T$ denotes the measurable state, $\mathbf{G}_1 = \text{diag}\,[1, -1]$, $\theta_1 = [\Delta C_X, \Delta C_Y, \Delta C_Z]^T$ and $\theta_2 = [\Delta C_l, \Delta C_m, \Delta C_n]^T$ are constant parameter uncertainties, $\bar{\omega} = [q_s, r_s]^T$ represents the intermediate control variable, $u = [\delta_a, \delta_e, \delta_r, \delta_{yl}, \delta_{yr}, \delta_{zl}, \delta_{zr}]^T$ denotes the control input, and $\mathbf{f}_1(\mathbf{x}), \mathbf{f}_2(\mathbf{x}), \mathbf{W}_1(\mathbf{x}), \mathbf{W}_2(\mathbf{x}), \mathbf{G}_2(\sigma), \mathbf{D}_1(\sigma), \mathbf{D}_2(\sigma)$ are vectors or matrices with appropriate dimensions (see appendix).

First of all, related assumptions used in the subsequent developments are given below.

Assumption 1. The desired trajectories $\alpha_d, \beta_d, p_{sd}$ and their derivatives are bounded. The compact set is defined as follows:

$$\Omega_1 = \left\{ (\alpha_d, \beta_d, p_{sd}) \middle| |\alpha_d| + |\beta_d| + |p_{sd}| + |\dot{\alpha}_d| + \left|\dot{\beta}_d\right| + |\dot{p}_{sd}| < \varpi \right\}, \tag{6}$$

where ϖ is a known positive constant and $|\cdot|$ stands for the absolute value of a scalar.

Assumption 2. For matrices $\mathbf{W}_1(x), \mathbf{W}_2(x), \mathbf{D}_1(\sigma), \mathbf{D}_2(\sigma)$, there exist positive constants $\tau_{1i}, \tau_{2i}, \tau_{3i}, \rho_{1i}, \rho_{2i} > 0, i = 1, 2$, such that $\|\mathbf{W}_i(\mathbf{x})\| \le \tau_{1i}$, $\|\dot{\mathbf{W}}_i(\mathbf{x})\| \le \tau_{2i}$, $\|\ddot{\mathbf{W}}_i(\mathbf{x})\| \le \tau_{3i}$, $\|\mathbf{D}_i(\sigma)\| \le \rho_{1i}$, $\|\dot{\mathbf{D}}_i(\sigma)\| \le \rho_{2i}, \forall \mathbf{x} \in \Omega_2$ with compact subset Ω_2 containing the origin, and $\|\cdot\|$ means the two norms of a vector or matrix.

To achieve precise reconstruction of unsteady states, a state filter is first introduced:

$$\begin{cases} \dot{\widehat{\sigma}} = \mathbf{f}_1(\mathbf{x}) + \mathbf{W}_1(\mathbf{x})\widehat{\eta} + \mathbf{G}_1\bar{\omega} + \mathbf{D}_1(\sigma)\widehat{\theta}_1 - \mathbf{K}_1 z_1, \\ \dot{\widehat{\omega}} = \mathbf{f}_2(\mathbf{x}) + \mathbf{W}_2(\mathbf{x})\widehat{\eta} + \mathbf{G}_2(\sigma)u + \mathbf{D}_2(\sigma)\widehat{\theta}_2 - \mathbf{K}_2 z_2, \end{cases} \tag{7}$$

where $\mathbf{K}_1, \mathbf{K}_2$ are positive definite matrices to be designed, $\widehat{\eta}$ denotes the estimate of η, $z_1 = \widehat{\sigma} - \sigma, z_2 = \widehat{\omega} - \omega$ are filter errors, and $\widehat{\theta}_1, \widehat{\theta}_2$ are estimates of θ_1, θ_2, respectively. According to (5) and (7), dynamics of z_1, z_2 take the form as

$$\begin{cases} \dot{z}_1 = \mathbf{W}_1(\mathbf{x})\tilde{\eta} + \mathbf{D}_1(\sigma)\tilde{\theta}_1 - \mathbf{K}_1 z_1, \\ \dot{z}_2 = \mathbf{W}_2(\mathbf{x})\tilde{\eta} + \mathbf{D}_2(\sigma)\tilde{\theta}_2 - \mathbf{K}_2 z_2, \end{cases} \tag{8}$$

where $\tilde{\eta} = \widehat{\eta} - \eta$ denotes the reconstruction error, $\tilde{\theta}_1 = \widehat{\theta}_1 - \theta_1$ and $\tilde{\theta}_2 = \widehat{\theta}_2 - \theta_2$ are estimate errors of uncertain parameters.

The state observer based on I&I theory is proposed as follows:

$$\widehat{\eta} = \varphi_0 + \mu_0[z, \mathbf{W}(\mathbf{x})], \tag{9}$$

where φ_0 denotes the observer state, $\mu_0[z, \mathbf{W}(\mathbf{x})]$ is a smooth nonlinear function, $z = [z_1^T, z_2^T]^T$, $\mathbf{W}(\mathbf{x}) = [\mathbf{W}_1^T(\mathbf{x}), \mathbf{W}_2^T(\mathbf{x})]^T$. Taking the time derivative of $\tilde{\eta}$ and using (8), we can get

$$\begin{aligned} \dot{\tilde{\eta}} = \dot{\varphi}_0 &+ \sum_{i=1}^{2} \frac{\partial \mu_0[z, \mathbf{W}(\mathbf{x})]}{\partial z_i} \left[\mathbf{W}_i(\mathbf{x})\tilde{\eta} + \mathbf{D}_i(\sigma)\tilde{\theta}_i - \mathbf{K}_i z_i \right] \\ &+ \sum_{i=1}^{2} \frac{\partial \mu_0[z, \mathbf{W}(\mathbf{x})]}{\partial \mathbf{W}_i(\mathbf{x})} \dot{\mathbf{W}}_i(\mathbf{x}) - h(x) + \mathbf{B}(\sigma)\eta. \end{aligned} \tag{10}$$

The nonlinear function $\mu_0[z, \mathbf{W}(\mathbf{x})]$ is selected so that $\tilde{\eta}$ has a stable behavior. So we choose

$$\begin{cases} \dfrac{\partial \mu_0[z, \mathbf{W}(\mathbf{x})]}{\partial z_1} = -\gamma_0 \mathbf{W}_1^T(\mathbf{x}), \\ \dfrac{\partial \mu_0[z, \mathbf{W}(\mathbf{x})]}{\partial z_2} = -\gamma_0 \mathbf{W}_2^T(\mathbf{x}), \end{cases} \tag{11}$$

with $\gamma_0 > 0$. Therefore, the nonlinear function is selected as

$$\mu_0[z, \mathbf{W}(\mathbf{x})] = -\gamma_0 \mathbf{W}_1^T(\mathbf{x}) z_1 - \gamma_0 \mathbf{W}_2^T(\mathbf{x}) z_2. \tag{12}$$

Then, substituting (12) into (10), we obtain

$$\begin{aligned} \dot{\tilde{\eta}} = \dot{\varphi}_0 &- \gamma_0 \sum_{i=1}^{2} \mathbf{W}_i^T(\mathbf{x}) \left[\mathbf{W}_i(\mathbf{x})\tilde{\eta} + \mathbf{D}_i(\sigma)\tilde{\theta}_i - \mathbf{K}_i z_i \right] \\ &- \sum_{i=1}^{2} \gamma_0 \dot{\mathbf{W}}_i^T(\mathbf{x}) z_i - h(x) + \mathbf{B}(\sigma)\eta. \end{aligned} \tag{13}$$

In (13), $\dot{\mathbf{W}}_i(\mathbf{x})$ contains the immeasurable state η and uncertain parameters θ_1, θ_2 which cannot be used directly. To overcome these difficulties, a command filter is employed to provide filtered derivative of $\mathbf{W}_i(\mathbf{x})$; the filter dynamics is expressed by

$$\ddot{\bar{\mathbf{W}}}_i(\mathbf{x}) + 2\varsigma\omega_n \dot{\bar{\mathbf{W}}}_i(\mathbf{x}) + \omega_n^2 \bar{\mathbf{W}}_i(\mathbf{x}) = \omega_n^2 \mathbf{W}_i(\mathbf{x}), \tag{14}$$

in which the initial condition satisfies $\bar{\mathbf{W}}_i[\mathbf{x}(0)] = \mathbf{W}_i[\mathbf{x}(0)]$, $\dot{\bar{\mathbf{W}}}_i[\mathbf{x}(0)] = 0$. Based on (13) and (14), the adaptation law is designed as

$$\dot{\varphi}_0 = \gamma_0 \sum_{i=1}^{2} \left[\dot{\mathbf{W}}_i^T(\mathbf{x}) z_i - \mathbf{W}_i^T(\mathbf{x}) \mathbf{K}_i z_i - \mathbf{W}_i^T(\mathbf{x}) z_i \right] + h(x) - \mathbf{B}(\sigma)\widehat{\eta}. \tag{15}$$

Substituting (15) into (13), we can get

$$\begin{aligned} \dot{\tilde{\eta}} = -\gamma_0 \sum_{i=1}^{2} \Big[&\mathbf{W}_i^T(\mathbf{x}) \mathbf{W}_i(\mathbf{x})\tilde{\eta} + \mathbf{W}_i^T(\mathbf{x}) \mathbf{D}_i(\sigma)\tilde{\theta}_i \\ &- \Delta\dot{\mathbf{W}}_i^T(\mathbf{x}) z_i + \mathbf{W}_i^T(\mathbf{x}) z_i \Big] - \mathbf{B}(\sigma)\tilde{\eta}, \end{aligned} \tag{16}$$

in which $\Delta\dot{\mathbf{W}}_i(\mathbf{x}) = \dot{\mathbf{W}}_i(\mathbf{x}) - \dot{\mathbf{W}}_i(\mathbf{x})$. According to Assumption 2, there exists a positive constant κ which depends on $\tau_{21}, \tau_{31}, \tau_{22}, \tau_{32}, \varsigma, \omega_n$ such that $\|\Delta\dot{\mathbf{W}}_1(\mathbf{x})\| \le \kappa$, $\|\Delta\dot{\mathbf{W}}_2(\mathbf{x})\| \le \kappa$ [39].

Consider the following Lyapunov function candidate

$$V_1 = \frac{1}{2}\gamma_0^{-1}\tilde{\eta}^T\tilde{\eta} + \frac{1}{2}z_1^T z_1 + \frac{1}{2}z_2^T z_2. \tag{17}$$

Using (8) and (16), the time derivative of V_1 yields

$$\dot{V}_1 = -\sum_{i=1}^{2}\Big[\tilde{\eta}^T\mathbf{W}_i^T(\mathbf{x})\mathbf{W}_i(\mathbf{x})\tilde{\eta} + \tilde{\eta}^T\mathbf{W}_i^T(\mathbf{x})\mathbf{D}_i(\sigma)\widetilde{\theta}_i - \tilde{\eta}^T\Delta\dot{\mathbf{W}}_i^T(\mathbf{x})z_i + z_i^T\mathbf{K}_i z_i - z_i^T D_i(\sigma)\widetilde{\theta}_i\Big] - \gamma_0^{-1}\tilde{\eta}^T\mathbf{B}(\sigma)\tilde{\eta}. \tag{18}$$

Using Young's inequality, we can get

$$\tilde{\eta}^T\mathbf{W}_i^T(\mathbf{x})\mathbf{D}_i(\sigma)\widetilde{\theta}_i \le a_1\|\mathbf{W}_i(\mathbf{x})\tilde{\eta}\|^2 + \frac{1}{4a_1}\left\|\mathbf{D}_i(\sigma)\widetilde{\theta}_i\right\|^2,$$

$$\tilde{\eta}^T\Delta\dot{\mathbf{W}}_i^T(\mathbf{x})z_i \le \|z_i\|\left\|\Delta\dot{\mathbf{W}}_i(\mathbf{x})\tilde{\eta}\right\| \le a_2\|z_i\|^2 + \frac{\kappa^2}{4a_2}\|\tilde{\eta}\|^2,$$

$$z_i^T\mathbf{D}_i(\sigma)\widetilde{\theta}_i \le a_3\|z_i\|^2 + \frac{1}{4a_3}\left\|\mathbf{D}_i(\sigma)\widetilde{\theta}_i\right\|^2, \tag{19}$$

where $a_1 \in (0, 1)$, $a_2, a_3 > 0$. Then, (18) is modified as

$$\begin{aligned}\dot{V}_1 \le{}& -(1-a_1)\|\mathbf{W}(\mathbf{x})\tilde{\eta}\|^2 - \left\{\gamma_0^{-1}\lambda_{\min}\mathbf{B}(\sigma) - \frac{\kappa^2}{2a_2}\right\}\|\tilde{\eta}\|^2 \\ &- [\lambda_{\min}(\mathbf{K}_1) - a_2 - a_3]\|z_1\|^2 - [\lambda_{\min}(\mathbf{K}_2) - a_2 - a_3]\|z_2\|^2 \\ &+ \left(\frac{1}{4a_1} + \frac{1}{4a_3}\right)\left\|\mathbf{D}_1(\sigma)\widetilde{\theta}_1\right\|^2 + \left(\frac{1}{4a_1} + \frac{1}{4a_3}\right)\left\|\mathbf{D}_2(\sigma)\widetilde{\theta}_2\right\|^2,\end{aligned} \tag{20}$$

with $\|\mathbf{W}(\mathbf{x})\tilde{\eta}\|^2 = \|\mathbf{W}_1(\mathbf{x})\tilde{\eta}\|^2 + \|\mathbf{W}_2(\mathbf{x})\tilde{\eta}\|^2$ and $\lambda_{\min}(\cdot)$ is the minimum eigenvalue of matrix. Note if $\mathbf{D}_1(\sigma)\widetilde{\theta}_1 = \mathbf{D}_2(\sigma)\widetilde{\theta}_2 = 0$ and the following inequalities hold

$$\begin{cases}\gamma_0^{-1}\lambda_{\min}\mathbf{B}(\sigma) - \dfrac{\kappa^2}{2a_2} > 0, \\ \min\{\lambda_{\min}(\mathbf{K}_1), \lambda_{\min}(\mathbf{K}_2)\} > a_2 + a_3,\end{cases} \tag{21}$$

then $\dot{V}_1 \le 0$, which implies that the state observation process is asymptotically stable. In the following parameter estimation, $\widehat{\theta}_1, \widehat{\theta}_2$ will be determined to regulate $\mathbf{D}_1(\sigma)\widetilde{\theta}_1 = \mathbf{D}_2(\sigma)\widetilde{\theta}_2 = 0$.

Remark 3. The differences between the preceding studies [26, 27, 29–33] and this research lie in the following two aspects:

(1) The I&I approach adopted in this section is used to reconstruct the immeasurable and time-varying states

(2) The filtered derivative of the regressor matrix, instead of filtered regressor matrix itself, is employed to construct the observer to avoid solving PDE

4. Constraint Adaptive Backstepping Control

In this section, a constraint adaptive backstepping controller based on I&I method is developed. The control objective is to track the predefined trajectories in the presence of input constraints and parameter uncertainties.

4.1. Constraint Backstepping Control. The constraint backstepping control design procedure is initiated by defining the following tracking errors:

$$e_1 = \sigma - \sigma_r, \bar{e}_2 = \bar{\omega} - \bar{\omega}_r, \tag{22}$$

where $\sigma_r = [\alpha_r, \beta_r]^T$ is the reference trajectory generated by the desired command $\sigma_d = [\alpha_d, \beta_d]^T$ and $\bar{\omega}_r = [q_{sr}, r_{sr}]^T$ is the virtual control law produced by $\bar{\omega}_d = [q_{sd}, r_{sd}]^T$.

To eliminate the "explosion of term" problem, $\bar{\omega}_d$ is filtered via a command filter to provide $\bar{\omega}_r$ and $\dot{\bar{\omega}}_r$. The difference between $\bar{\omega}_r$ and $\bar{\omega}_d$ is evaluated by an auxiliary filter

$$\dot{\xi}_1 = -\mathbf{A}_1\xi_1 + \mathbf{G}_1(\bar{\omega}_r - \bar{\omega}_d) + \bar{\mathbf{G}}_1\xi_2, \tag{23}$$

where $\mathbf{A}_1 > 0$, $\bar{\mathbf{G}}_1 = (0_{2\times1}, \mathbf{G}_1)$, ξ_1 is the filter state, and ξ_2 will be defined later. The compensated errors are defined by

$$\varepsilon_1 = e_1 - \xi_1, \varepsilon_2 = e_2 - \xi_2, \tag{24}$$

where $e_2 = (p_s - p_{sr}, \bar{e}_2^T)^T$, and p_{sr} denotes the reference trajectory of stability axis roll rate generated by p_{sd}. Taking time derivative of e_1 and using (5), we obtain

$$\dot{e}_1 = \mathbf{f}_1(\mathbf{x}) + \mathbf{W}_1(\mathbf{x})\eta + \mathbf{D}_1(\sigma)\theta_1 - \dot{\sigma}_r + \mathbf{G}_1\bar{e}_2 + \mathbf{G}_1(\bar{\omega}_r - \bar{\omega}_d) + \mathbf{G}_1\bar{\omega}_d. \tag{25}$$

Therefore, the nominal virtual control law $\bar{\omega}_d$ is given by

$$\bar{\omega}_d = \mathbf{G}_1^{-1}\left[-\mathbf{f}_1(\mathbf{x}) - \mathbf{W}_1(\mathbf{x})\widehat{\eta} - \mathbf{D}_1(\sigma)\widehat{\theta}_1 + \dot{\sigma}_r - \mathbf{A}_1 e_1\right]. \tag{26}$$

Combining (23), (24), (25), and (26), the dynamics of ε_1 takes the form as

$$\dot{\varepsilon}_1 = -\mathbf{W}_1(\mathbf{x})\tilde{\eta} - \mathbf{D}_1(\sigma)\widetilde{\theta}_1 + \bar{\mathbf{G}}_1\varepsilon_2 - \mathbf{A}_1\varepsilon_1. \tag{27}$$

Similar to (26), the nominal control law u_d for angular rate subsystem is designed as

$$u_d = \mathbf{G}_2^{+}(\sigma)\left[-\mathbf{f}_2(\mathbf{x}) - \mathbf{W}_2(\mathbf{x})\widehat{\eta} - \mathbf{D}_2(\sigma)\widehat{\theta}_2 + \dot{\omega}_r - \mathbf{A}_2 e_2 - \bar{\mathbf{G}}_1^T\varepsilon_1\right], \tag{28}$$

where $\mathbf{G}_2^{+}(\sigma)$ is pseudoinverse of $\mathbf{G}_2(\sigma)$, $\dot{\omega}_r = (\dot{p}_{sr}, \dot{\bar{\omega}}_r^T)^T$, $\dot{p}_{sr}$ can be obtained by filtering p_{sd}.

To impose physical constraints on actuators, u_d is filtered via a command filter to provide the physical limited u. The command filter integrated with magnitude and rate limits is described as [14]

$$\ddot{u} = 2\varsigma\omega_n \left\{ S_R\left[\frac{\omega_n}{2\varsigma}\left(S_M(u_d) - u\right)\right] - \dot{u} \right\}, \tag{29}$$

where $S_M(\cdot), S_R(\cdot)$ are magnitude and rate saturation function, respectively. The impact of (29) can be evaluated by

$$\dot{\xi}_2 = -\mathbf{A}_2\xi_2 + \mathbf{G}_2(\sigma)(u - u_d), \tag{30}$$

where $A_2 > 0$. Combining (5), (24), (28), and (30), the dynamics of ε_2 is expressed by

$$\dot{\varepsilon}_2 = -\mathbf{W}_2(\mathbf{x})\tilde{\eta} - \mathbf{D}_2(\sigma)\tilde{\theta}_2 - \bar{\mathbf{G}}_1^T\varepsilon_1 - \mathbf{A}_2\varepsilon_2. \tag{31}$$

Then, the following Lyapunov function candidate is considered:

$$V_2 = \frac{1}{2}\varepsilon_1^T\varepsilon_1 + \frac{1}{2}\varepsilon_2^T\varepsilon_2. \tag{32}$$

Taking the time derivative of V_2 along (27) and (31) and using Young's inequality, we have

$$\begin{aligned}
\dot{V}_2 &= \varepsilon_1^T\left[-\mathbf{W}_1(\mathbf{x})\tilde{\eta} - \mathbf{D}_1(\sigma)\tilde{\theta}_1 + \bar{\mathbf{G}}_1\varepsilon_2 - \mathbf{A}_1\varepsilon_1\right] \\
&\quad + \varepsilon_2^T\left[-\mathbf{W}_2(\mathbf{x})\tilde{\eta} - \mathbf{D}_2(\sigma)\tilde{\theta}_2 - \bar{\mathbf{G}}_1^T\varepsilon_1 - \mathbf{A}_2\varepsilon_2\right] \\
&\le -[\lambda_{\min}(\mathbf{A}_1) - b_1 - b_3]\|\varepsilon_1\|^2 - [\lambda_{\min}(\mathbf{A}_2) - b_2 - b_4]\|\varepsilon_2\|^2 \\
&\quad + \frac{1}{4b_1}\|\mathbf{W}_1(\mathbf{x})\tilde{\eta}\|^2 + \frac{1}{4b_2}\|\mathbf{W}_2(\mathbf{x})\tilde{\eta}\|^2 \\
&\quad + \frac{1}{4b_3}\left\|\mathbf{D}_1(\sigma)\tilde{\theta}_1\right\|^2 + \frac{1}{4b_4}\left\|\mathbf{D}_2(\sigma)\tilde{\theta}_2\right\|^2,
\end{aligned} \tag{33}$$

where $b_1, b_2, b_3, b_4 > 0$.

4.2. Uncertain Parameter Estimation. Now the design of the parameter estimator is considered. This process is completed by deriving the nonlinear functions and adaptation laws for partial estimates.

The estimator of θ_1 based on the I&I approach is constructed as

$$\hat{\theta}_1 = \varphi_1 + \mu_1[\varepsilon_1, \mathbf{D}_1(\sigma)], \tag{34}$$

where φ_1 is the partial estimate of θ_1 and $\mu_1[\varepsilon_1, \mathbf{D}_1(\sigma)]$ denotes the nonlinear function of ε_1 and $\mathbf{D}_1(\sigma)$. Taking the time derivative of $\hat{\theta}_1$ and combining (27), we can get

$$\begin{aligned}
\dot{\tilde{\theta}}_1 &= \frac{\partial\mu_1[\varepsilon_1, \mathbf{D}_1(\sigma)]}{\partial\varepsilon_1}\left[-\mathbf{W}_1(\mathbf{x})\tilde{\eta} - \mathbf{D}_1(\sigma)\tilde{\theta}_1 + \bar{\mathbf{G}}_1\varepsilon_2 - \mathbf{A}_1\varepsilon_1\right] \\
&\quad + \left[\frac{\partial\mathbf{D}_1(\sigma)}{\partial\alpha}\dot{\alpha} + \frac{\partial\mathbf{D}_1(\sigma)}{\partial\beta}\dot{\beta}\right]^T\frac{\partial\mu_1[\varepsilon_1, \mathbf{D}_1(\sigma)]}{\partial\mathbf{D}_1(\sigma)} + \dot{\varphi}_1.
\end{aligned} \tag{35}$$

To ensure that $\tilde{\theta}_1$ has a stable behavior, the nonlinear function $\mu_1[\varepsilon_1, \mathbf{D}_1(\sigma)]$ is chosen as

$$\mu_1[\varepsilon_1, \mathbf{D}_1(\sigma)] = \gamma_1\mathbf{D}_1^T(\sigma)\varepsilon_1, \tag{36}$$

where $\gamma_1 > 0$. In view of (35) and (36), if φ_1 is updated by

$$\dot{\varphi}_1 = \gamma_1\mathbf{D}_1^T(\sigma)\left[-\bar{\mathbf{G}}_1\varepsilon_2 + \mathbf{A}_1\varepsilon_1\right] - \gamma_1\left[\frac{\partial\mathbf{D}_1(\sigma)}{\partial\alpha}\dot{\alpha} + \frac{\partial\mathbf{D}_1(\sigma)}{\partial\beta}\dot{\beta}\right]^T\varepsilon_1, \tag{37}$$

then substituting (37) into (35), we can get

$$\dot{\tilde{\theta}}_1 = -\gamma_1\mathbf{D}_1^T(\sigma)\mathbf{D}_1(\sigma)\tilde{\theta}_1 - \gamma_1\mathbf{D}_1^T(\sigma)\mathbf{W}_1(\mathbf{x})\tilde{\eta}. \tag{38}$$

For angular rate subsystem, the estimator of θ_2 is given as follows

$$\hat{\theta}_2 = \varphi_2 + \mu_2[\varepsilon_2, \mathbf{D}_2(\sigma)], \tag{39}$$

with

$$\mu_2[\varepsilon_2, \mathbf{D}_2(\sigma)] = \gamma_2\mathbf{D}_2^T(\sigma)\varepsilon_2, \tag{40}$$

$$\dot{\varphi}_2 = \gamma_2\mathbf{D}_2^T(\sigma)\left[\bar{\mathbf{G}}_1^T\varepsilon_1 + \mathbf{A}_2\varepsilon_2\right] - \gamma_2\left[\frac{\partial\mathbf{D}_2(\sigma)}{\partial\alpha}\dot{\alpha} + \frac{\partial\mathbf{D}_2(\sigma)}{\partial\beta}\dot{\beta}\right]^T\varepsilon_2, \tag{41}$$

where $\gamma_2 > 0$. Combining (39), (40), and (41), the dynamics of $\tilde{\theta}_2$ can be expressed by

$$\dot{\tilde{\theta}}_2 = -\gamma_2\mathbf{D}_2^T(\sigma)\mathbf{D}_2(\sigma)\tilde{\theta}_2 - \gamma_2\mathbf{D}_2^T(\sigma)\mathbf{W}_2(\mathbf{x})\tilde{\eta}. \tag{42}$$

Define the Lyapunov function candidate

$$V_3 = \frac{1}{2}\gamma_1^{-1}\tilde{\theta}_1^T\tilde{\theta}_1 + \frac{1}{2}\gamma_2^{-1}\tilde{\theta}_2^T\tilde{\theta}_2. \tag{43}$$

Differentiating V_3 and invoking (38) and (42), we have

$$\begin{aligned}
\dot{V}_3 &= -\sum_{i=1}^{2}\left[\tilde{\theta}_i^T\mathbf{D}_i^T(\sigma)\mathbf{D}_i(\sigma)\tilde{\theta}_i + \tilde{\theta}_i^T\mathbf{D}_i^T(\sigma)\mathbf{W}_i(\mathbf{x})\tilde{\eta}\right] \\
&\le -(1 - b_1)\left\|\mathbf{D}_1(\sigma)\tilde{\theta}_1\right\|^2 - (1 - b_2)\left\|\mathbf{D}_2(\sigma)\tilde{\theta}_2\right\|^2 \\
&\quad + \frac{1}{4b_1}\|\mathbf{W}_1(\mathbf{x})\tilde{\eta}\|^2 + \frac{1}{4b_2}\|\mathbf{W}_2(\mathbf{x})\tilde{\eta}\|^2.
\end{aligned} \tag{44}$$

Remark 4. Assume that the state observer performs perfectly in reconstructing the unsteady states, then $\tilde{\eta} = 0$ can be achieved. Hence, according to (38), the dynamics of $\tilde{\theta}_1$ can be treated as a linear time-varying system given by $\dot{\tilde{\theta}}_1(t) = -\gamma_1\mathbf{D}_1^T[\sigma(t)]\mathbf{D}_1[\sigma(t)]\tilde{\theta}_1(t)$. Note that if at some instant t_1, $\tilde{\theta}_1(t_1) = 0$, then $\tilde{\theta}_1(t) = \mathbf{0}$ for $t \ge t_1$. That is, the manifold defined by $\Omega_3 = \{(x, \eta, t)|\varphi_1 + \mu_1[\varepsilon_1, \mathbf{D}_1(\sigma)] - \theta_1 = 0\}$ is an invariant manifold. Therefore, the parameter estimate $\varphi_1 + \mu_1[\varepsilon_1, \mathbf{D}_1(\sigma)]$ remains frozen at its actual value for $t \ge t_1$. This invariant characteristic also holds for $\tilde{\theta}_2$ dynamics.

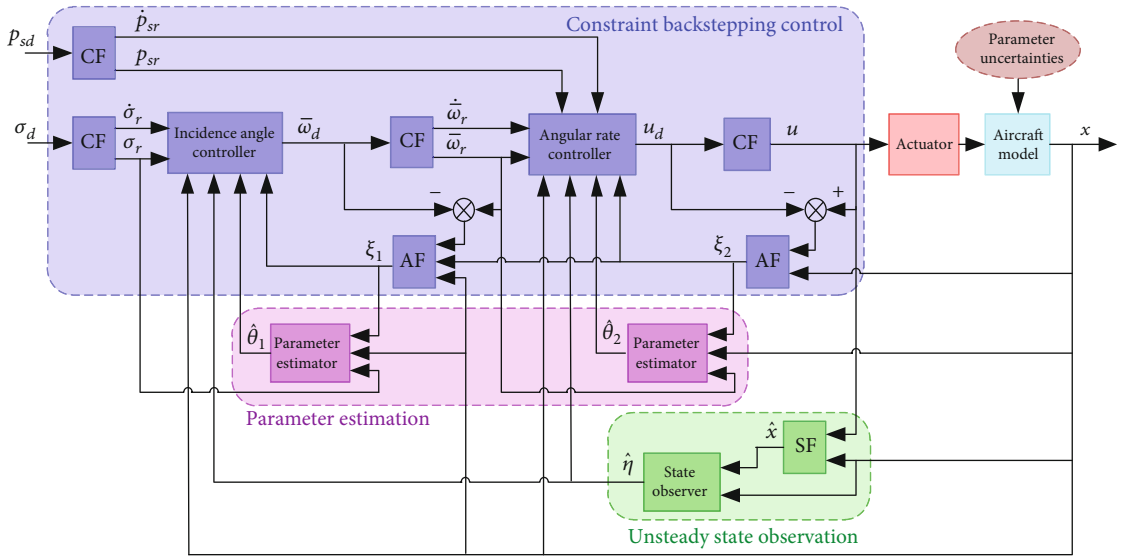

AF: auxiliary filter, CF: command filter, SF: state filter

Figure 2: Overview of the control system architecture.

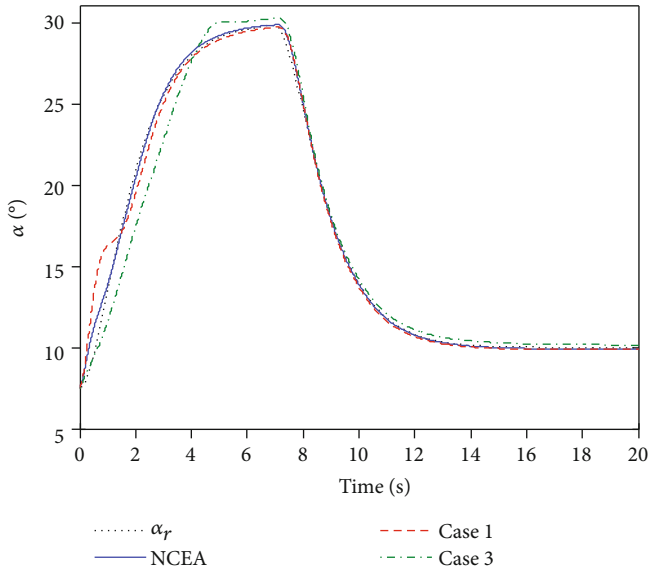

Figure 3: Time history of the command tracking.

Remark 5. Note that availability of $\dot{\alpha}, \dot{\beta}$ is assumed in the estimator design; otherwise, we will need to solve PDE. Although $\dot{\alpha}, \dot{\beta}$ cannot be measured directly, we could attempt to compute via velocity components and incidence angles.

Remark 6. According to (38) and (42), we can find that the state reconstruction error $\tilde{\eta}$ may affect the estimator performance, that is to say, the observer and estimator are coupled together. To weaken the effects between each other, the design parameters of the observer and estimator need to be chosen appropriately. In practice, the reconstruction error $\tilde{\eta}$ should converge much more quickly than the estimate errors $\widetilde{\theta}_1, \widetilde{\theta}_2$ to satisfy the spectrum separation principle.

4.3. Stability Analysis. The stability analysis of closed-loop system is initiated by the following theorem.

Theorem 7. *Consider the closed-loop system under the foregoing assumptions, with application of the state filter (7), state observer (9), constraint backstepping controller (26) and (28), and the parameter estimator (34) and (39),* $\mathbf{W}(\mathbf{x})\tilde{\eta}, \tilde{\eta}$, $z_1, z_2, \varepsilon_1, \varepsilon_2, \mathbf{D}_1(\sigma)\widetilde{\theta}_1, \mathbf{D}_2(\sigma)\widetilde{\theta}_2$ *can be guaranteed to converge to zero.*

Proof. The Lyapunov function is chosen as

$$V_4 = V_1 + V_2 + V_3. \tag{45}$$

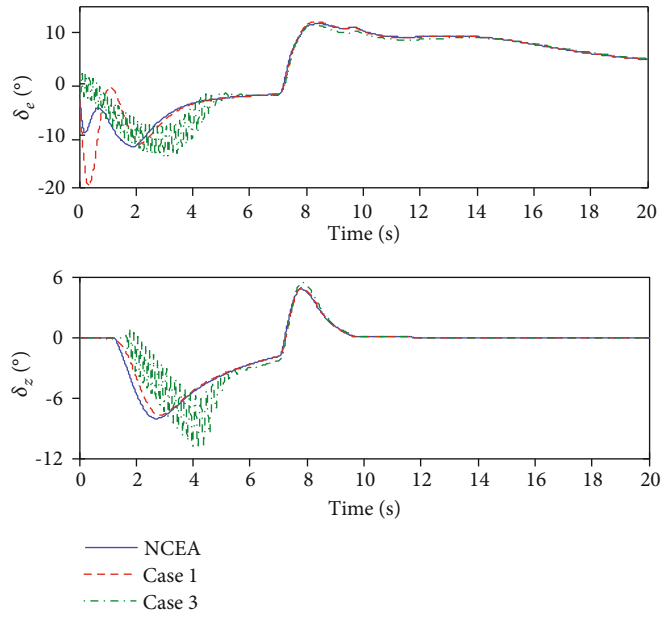

Figure 4: Time histories of the control inputs.

Combining (20), (33), and (44), the time derivative of V_4 yields

$$\begin{aligned}\dot{V}_4 \le & -(1-a_1)\|\mathbf{W}(\mathbf{x})\tilde{\eta}\|^2 - \left\{\gamma_0^{-1}\lambda_{\min}\mathbf{B}(\sigma) - \frac{\kappa^2}{2a_2} - \frac{\tau_{11}^2}{2b_1} - \frac{\tau_{12}^2}{2b_2}\right\}\|\tilde{\eta}\|^2 \\ & - [\lambda_{\min}(\mathbf{K}_1) - a_2 - a_3]\|z_1\|^2 - [\lambda_{\min}(\mathbf{K}_2) - a_2 - a_3]\|z_2\|^2 \\ & - [\lambda_{\min}(\mathbf{A}_1) - b_1 - b_3]\|\varepsilon_1\|^2 - [\lambda_{\min}(\mathbf{A}_2) - b_2 - b_4]\|\varepsilon_2\|^2 \\ & - \left(1 - b_1 - \frac{1}{4a_1} - \frac{1}{4a_3} - \frac{1}{4b_3}\right)\left\|\mathbf{D}_1(\sigma)\tilde{\theta}_1\right\|^2 \\ & - \left(1 - b_2 - \frac{1}{4a_1} - \frac{1}{4a_3} - \frac{1}{4b_4}\right)\left\|\mathbf{D}_2(\sigma)\tilde{\theta}_2\right\|^2.\end{aligned} \tag{46}$$

To ensure stability of the closed-loop system, we select appropriate matrices $\mathbf{A}_1, \mathbf{A}_2, \mathbf{K}_1, \mathbf{K}_2$ and adaptation gain γ_0 to satisfy the following inequalities:

$$\begin{aligned}&\gamma_0^{-1}\lambda_{\min}\mathbf{B}(\sigma) > \frac{\kappa^2}{2a_2} + \frac{\tau_{11}^2}{2b_1} + \frac{\tau_{12}^2}{2b_2}, \\ &\lambda_{\min}(\mathbf{A}_1) > b_1 + b_3, \lambda_{\min}(\mathbf{A}_2) > b_2 + b_4, \\ &b_1 + \frac{1}{4a_1} + \frac{1}{4a_3} + \frac{1}{4b_3} < 1, b_2 + \frac{1}{4a_1} + \frac{1}{4a_3} + \frac{1}{4b_4} < 1,\end{aligned} \tag{47}$$

and inequalities (21), then $\dot{V}_4 \le 0$ can be achieved. Thus, we can conclude that all closed-loop signals are bounded based on Assumptions 1 and 2. Further, because V_4 is lower-bounded and monotonic by the negative-semidefiniteness of $\dot{V}_4$, we know that $\int_0^\infty \dot{V}_4(t)dt$ exists and is finite, which in turn implies

$$\left[\mathbf{W}(\mathbf{x})\tilde{\eta}, \tilde{\eta}, z_1, z_2, \varepsilon_1, \varepsilon_2, \mathbf{D}_1(\sigma)\tilde{\theta}_1, \mathbf{D}_2(\sigma)\tilde{\theta}_2\right] \in L_2 \cap L_\infty. \tag{48}$$

Since $\mathbf{W}(\mathbf{x}), \mathbf{D}_1(\sigma), \mathbf{D}_2(\sigma)$ and their derivatives are all bounded, according to Barbalat's lemma, it follows that

$$\lim_{t\to\infty}\left[\mathbf{W}(\mathbf{x})\tilde{\eta}, \tilde{\eta}, z_1, z_2, \varepsilon_1, \varepsilon_2, \mathbf{D}_1(\sigma)\tilde{\theta}_1, \mathbf{D}_2(\sigma)\tilde{\theta}_2\right] = 0. \tag{49}$$

Thus, $\mathbf{W}(\mathbf{x})\tilde{\eta}, \tilde{\eta}, z_1, z_2, \varepsilon_1, \varepsilon_2, \mathbf{D}_1(\sigma)\tilde{\theta}_1, \mathbf{D}_2(\sigma)\tilde{\theta}_2$ can be guaranteed to converge to zero.

According to Theorem 7, $\mathbf{W}(\mathbf{x})\tilde{\eta}, \mathbf{D}_1(\sigma)\tilde{\theta}_1, \mathbf{D}_2(\sigma)\tilde{\theta}_2$ asymptotically converges to zero. Thus, the manifold defined by

$$\Omega_7 = \Omega_1 \cap \Omega_2 \cap \Omega_4 \cap \Omega_5 \cap \Omega_6, \tag{50}$$

with

$$\begin{aligned}\Omega_4 &= \{\mathbf{W}(\mathbf{x})(\varphi_0 + \mu_0[z, \mathbf{W}(\mathbf{x})] - \eta) = 0\}, \\ \Omega_5 &= \{\mathbf{D}_1(\sigma)(\varphi_1 + \mu_1[\varepsilon_1, \mathbf{D}_1(\sigma)] - \theta_1) = 0\}, \\ \Omega_6 &= \{\mathbf{D}_2(\sigma)(\varphi_2 + \mu_2[\varepsilon_2, \mathbf{D}_2(\sigma)] - \theta_2) = 0\},\end{aligned} \tag{51}$$

is an attractive manifold. Along any trajectories evolving on Ω_7, the dynamics of $\varepsilon_1, \varepsilon_2$can be described by

$$\begin{cases}\dot{\varepsilon}_1 = \bar{\mathbf{G}}_1\varepsilon_2 - \mathbf{A}_1\varepsilon_1, \\ \dot{\varepsilon}_2 = -\bar{\mathbf{G}}_1^T\varepsilon_1 - \mathbf{A}_2\varepsilon_2.\end{cases} \tag{52}$$

Apparently, (52) can be obtained if a controller based on attitude dynamics with measurable unsteady states and known aerodynamic parameters is implemented. Hence,

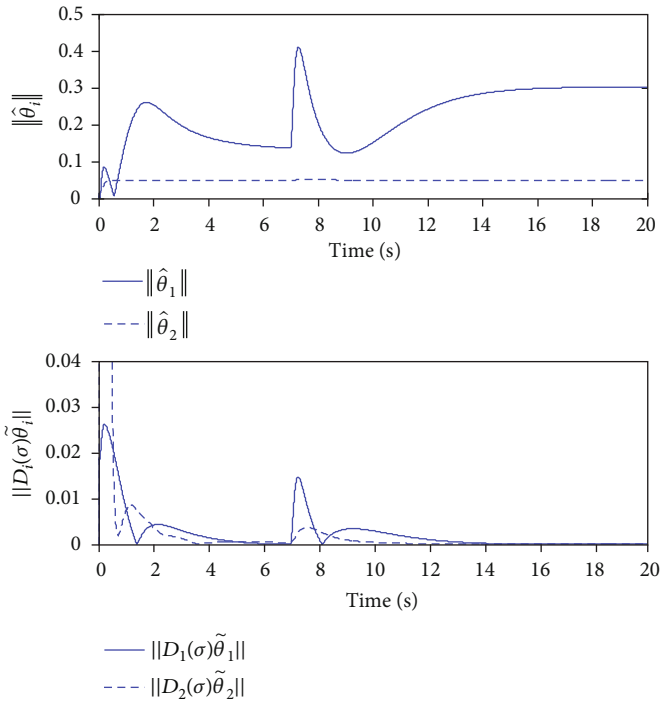

Figure 5: Time histories of the norms.

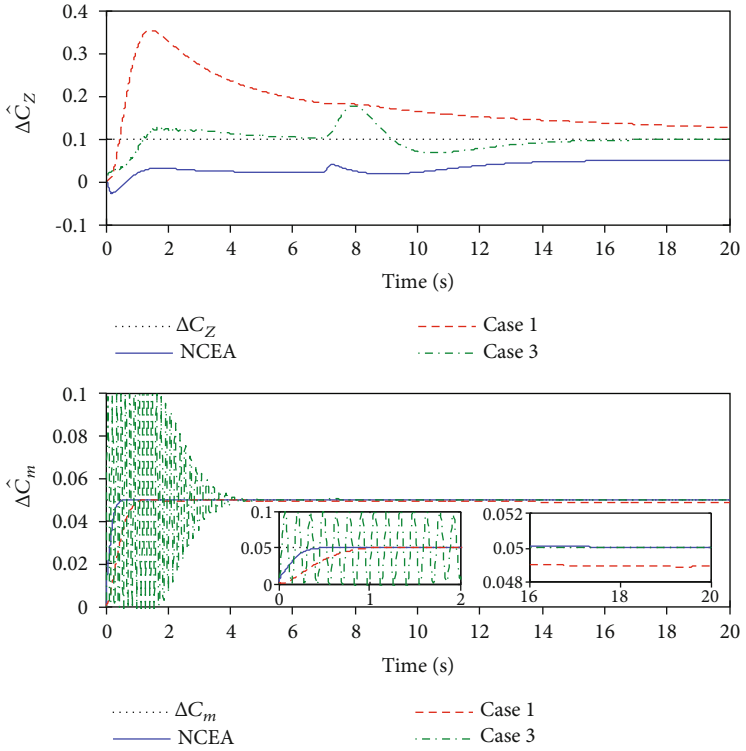

Figure 6: Estimation of the uncertain parameters.

Table 2: The performance indexes of the NCEA and CEA laws.

Methods	RMSE (°)	Maximum error (°)	EC (J)	Maximum δ_e (°)	Maximum δ_z (°)
NCEA	0.3205	1.65	2.53×10^5	12.15	8.05
CEA					
Case 1	0.8126	4.18	2.64×10^5	19.75	7.72
Case 2	0.4486	2.10	2.75×10^5	13.80	8.50
Case 3	1.120	3.45	5.55×10^5	14.05	10.9

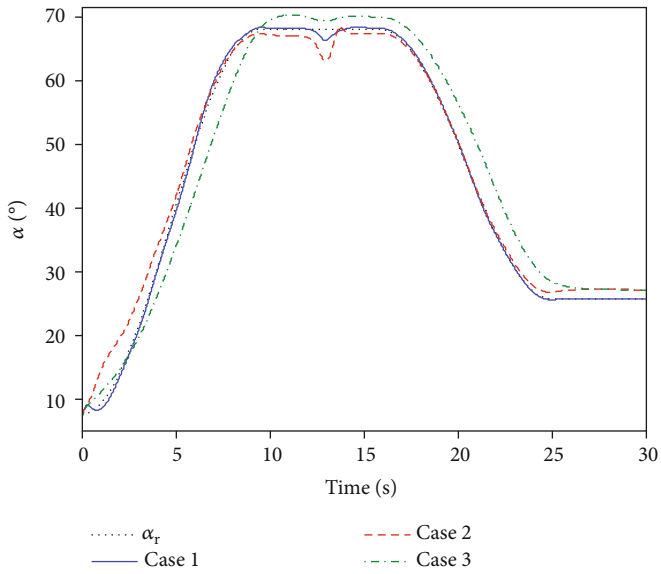

Figure 7: Time history of the longitudinal command tracking.

the constraint backstepping controllers (26) and (28) capture the performance of the deterministic control system. From (52), it can be easily seen

$$\dot{V}_2 = -\varepsilon_1^T \mathbf{A}_1 \varepsilon_1 - \varepsilon_2^T \mathbf{A}_2 \varepsilon_2 \leq -\lambda_{\min}(\mathbf{A}_1)\|\varepsilon_1\|^2 - \lambda_{\min}(\mathbf{A}_2)\|\varepsilon_2\|^2, \tag{53}$$

which implies that $\varepsilon_1, \varepsilon_2$ will converge to zero as expected.

Remark 8. For the closed-loop stability analysis, two scenarios are considered:

(1) When actuator constraints are not in effect, note the fact that $\bar{\omega}_r - \bar{\omega}_d$ and $u - u_d$ are bounded, then the auxiliary filter states ξ_1, ξ_2 converge to a sufficient small domain around origin by selecting appropriate natural angular frequency ω_n and control matrices $\mathbf{A}_1, \mathbf{A}_2$. Therefore, from (24), it is obvious that the tracking errors e_1, e_2 can be guaranteed to be bounded. Consequently, the stability of the closed-loop system can be ensured

(2) When input saturation occurs, the primary control object is to maintain the stability of online approximation process [14]. It is obvious that the tracking errors may increase while the compensated errors still converge to zero when saturation happens. Through replacing the tracking errors by compensated errors in the parameter estimation, the stability of the adaptation process can be ensured not affected by the saturation

In conclusion, the proposed control scheme consists of three modules: unsteady states observation, constraint backstepping control, and parameter estimation. The overview of the design architecture is depicted in Figure 2.

5. Numerical Simulations and Discussions

This section presents several numerical simulations which are carried out to investigate the performance of the proposed control scheme. The comparisons of the NCEA and CEA laws are completed in the first simulation. The second simulation is performed to examine the effectiveness of the proposed control scheme via the Herbst maneuver. Both the simulations are conducted in the MATLAB/Simulink environment, where the step size is set to 5 ms. The parameters of the fighter are given in [36].

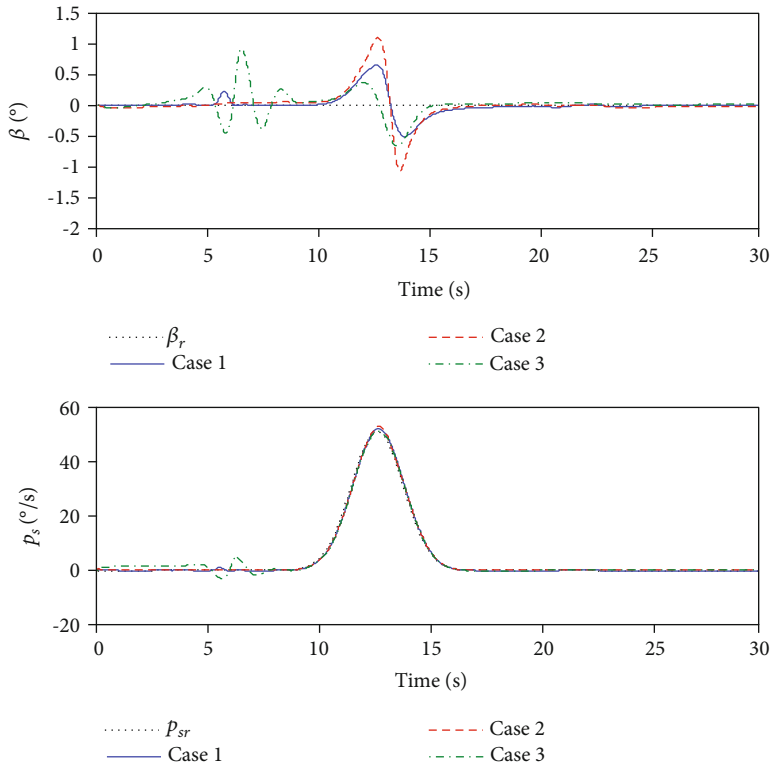

Figure 8: Time histories of the lateral command tracking.

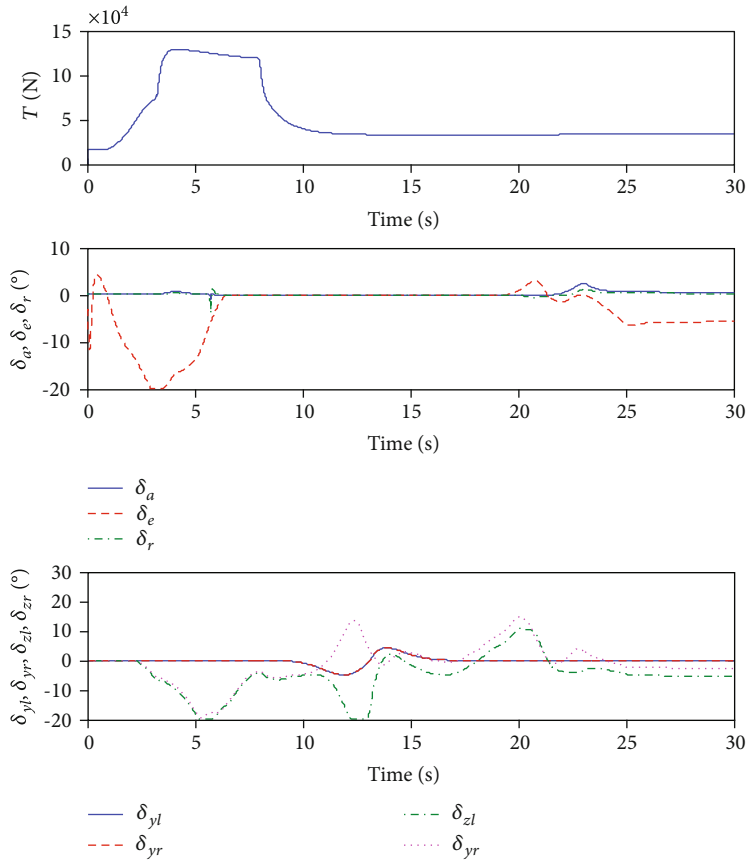

Figure 9: Time histories of the control inputs.

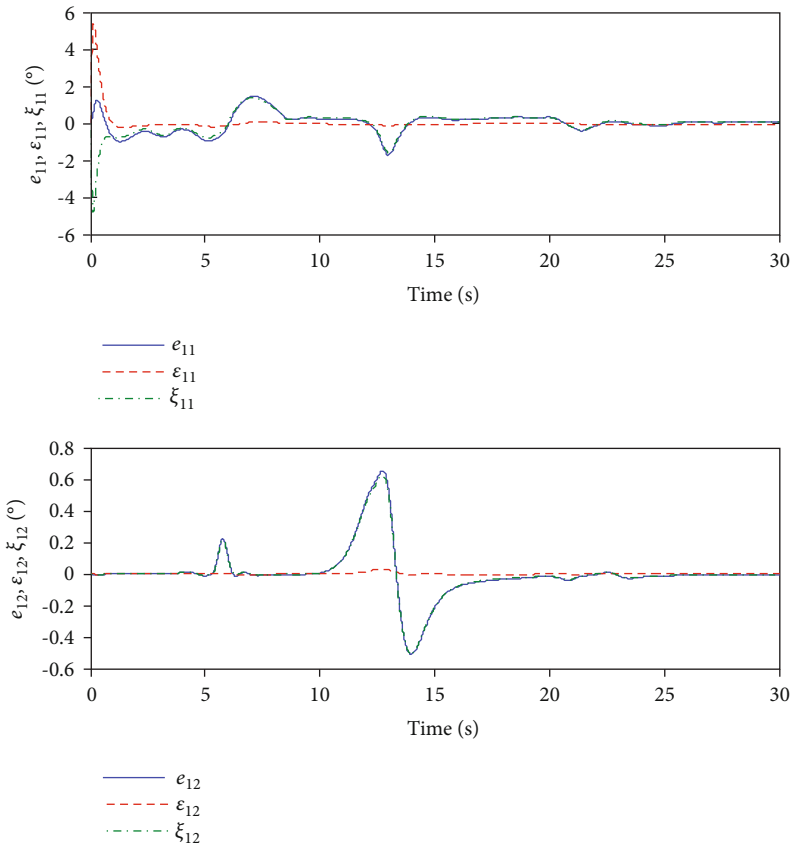

Figure 10: Related errors in angular subsystem.

5.1. Comparisons of NCEA and CEA Laws. In this subsection, comparisons of the constraint filter backstepping controller based on the NCEA and CEA laws are performed to evaluate the adaptation effects on the closed-loop system. The parameters of the proposed controller are chosen as $\mathbf{K}_1 = \text{diag}\,[8, 8]$, $\mathbf{K}_2 = \text{diag}\,[20, 20, 20]$, $\mathbf{A}_1 = \text{diag}\,[3, 3]$, $\mathbf{A}_2 = \text{diag}\,[6, 6, 6]$, $\gamma_0 = 5 \times 10^{-3}$, $\gamma_1 = 1 \times 10^3$, $\gamma_2 = 2 \times 10^{-3}$, $\varsigma = 0.8$, $\omega_n = 30$ rad/s. The initial estimate values of the unsteady states and uncertain parameters are all set to zero. Besides the desired command of AOA, the commands of β, p_s are set to zero to neglect the lateral motion for simplicity. Meanwhile, parameter uncertainties are added into C_Z, C_m to simulate model errors. The equilibrium states at $\alpha = 7.50^\circ$ are chosen as the initial condition.

To illustrate the essence of the NCEA law, adaptive backstepping control approach proposed in [14] is adopted for comparison, the CEA laws are given as

$$\dot{\widehat{\eta}} = h(x) - \mathbf{B}(\sigma)\widehat{\eta} - \mathbf{W}^T(\mathbf{x})z,\ \dot{\widehat{\theta}}_1 = \gamma_3 \mathbf{D}_1^T(\sigma)\varepsilon_1,\ \dot{\widehat{\theta}}_2 = \gamma_4 \mathbf{D}_2^T(\sigma)\varepsilon_2, \tag{54}$$

where γ_3, γ_4 are adaptation gains to be assigned. Consider that the transient control performance is highly dependent on adaptation gains, four sets of gains with different adaptation rates are selected, that is,

Case 1. (slow): $\gamma_3 = 30,\ \gamma_4 = 0.003$.

Case 2. (medium): $\gamma_3 = 100,\ \gamma_4 = 0.01$.

Case 3. (fast): $\gamma_3 = 500,\ \gamma_4 = 0.3$.

In order to compare the performance of different adaptive laws, the root-mean-square (RSME) of tracking errors and the energy consumption (EC) are chosen as the evaluation indexes which are defined as

$$\text{RSME} = \sqrt{\frac{1}{n}\sum_{i=1}^{n}\left[\left(\alpha^i - \alpha_r^i\right)^2 + \left(\beta^i - \beta_r^i\right)^2 + \left(p_s^i - p_{sr}^i\right)^2\right]},$$
$$\text{EC} = \int_0^{t_f} \left(|L_c||p| + |M_c||q| + |N_c||r|\right) dt, \tag{55}$$

where the superscript i means the ith sampling point, n denotes the number of samples, t_f denotes the final time of simulation, and L_c, M_c, N_c are the commands of total control moment in each channel.

Simulation results are shown in Figures 3–6 and Table 2. It should be pointed out that the unsteady states are perfectly reconstructed with fast converge rates for both adaptive laws; therefore, the results are not presented herein. From Figures 3 and 4 and Table 2, it is apparent that the NCEA law outperforms the three CEA laws both in command tracking and energy consumption. The track performance of the

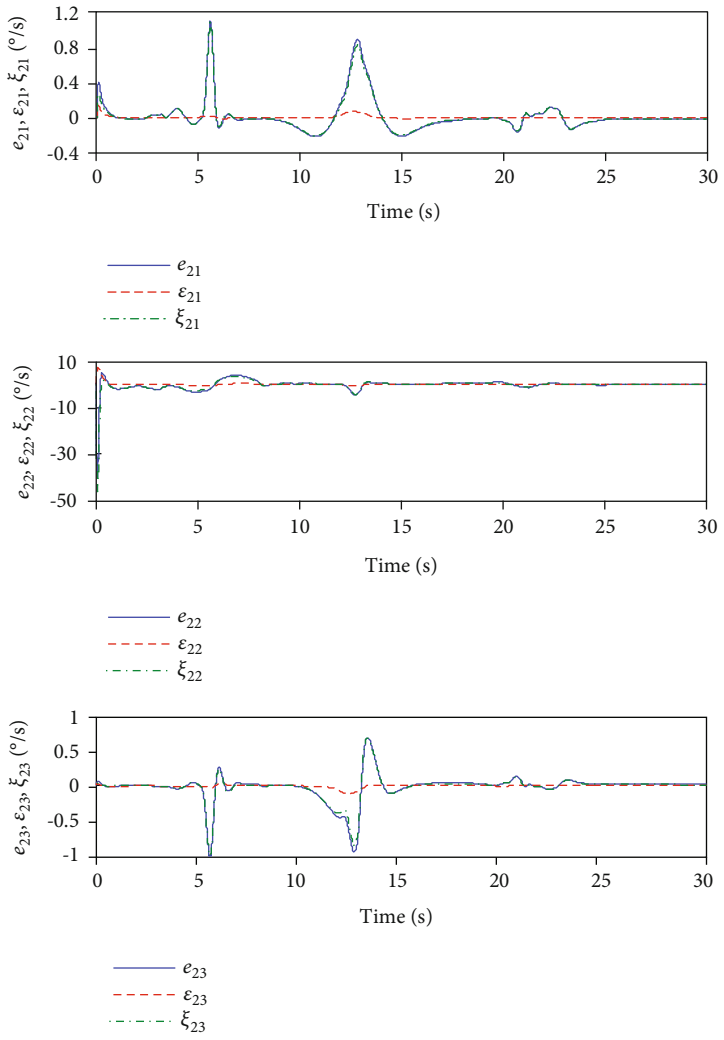

FIGURE 11: Related errors in angular rate subsystem.

CEA laws is sensitive to the adaptation gains. When compared with the case 1, the CEA law in case 3 achieves higher estimate precision and faster converging rate at the expense of sacrificing the energy consumption and transient control performance. It can be observed from Figure 5 that $\mathbf{D}_1(\sigma)\widetilde{\theta}_1$, $\mathbf{D}_2(\sigma)\widetilde{\theta}_2$ are converged to zero; thus, the closed-loop trajectory eventually confines to the manifold Ω_7, and the NCEA law recovers the performance of the deterministic backstepping controller. Figure 6 shows the time history of parameter estimation; it is obvious that the parameters estimated by CEA laws drift from their true values, especially in case 1. For the NCEA law, ΔC_m can be precisely estimated while this is not the case for ΔC_Z. The reason is that the rank of $\mathbf{D}_2(\sigma)$ equals to $\widetilde{\theta}_2$, then $\mathbf{D}_2(\sigma)\widetilde{\theta}_2 = 0$ means $\widetilde{\theta}_2 = 0$; therefore, the invariant manifold is achieved and θ_2 can be estimated accurately. However, the rank of $\mathbf{D}_1(\sigma)$ is less than $\widetilde{\theta}_1$; hence, $\widetilde{\theta}_1 = 0$ cannot be guaranteed via $\mathbf{D}_1(\sigma)\widetilde{\theta}_1 = 0$. In addition, it can be seen that $\widehat{\theta}_1$ is frozen after $t = 15$ s at which instant the attractive manifold $\mathbf{D}_1(\sigma)\widetilde{\theta}_1 = 0$ is achieved.

5.2. Robust Analysis under Parameter Uncertainties and Unsteady Effects. To justify the effectiveness of the proposed control scheme, three different cases are considered for comparison. In the first case, the controller proposed in Section 4 is adopted in which the effects of unsteady aerodynamics and uncertain parameters are both compensated. For the second case, the effects of uncertain parameters are not considered in the controller design. The third case is the worst case in which both the unsteady effects and uncertain parameters are not compensated. The design parameters of the controller and initial condition are all kept the same as that in the previous subsection. The uncertainties of aerodynamic forces and moments in longitudinal and lateral channels are all considered in this simulation. Moreover, the Herbst maneuver is implemented to validate the control performance; the commands of $\alpha_d, \beta_d, p_{sd}$ are defined in [35].

The commands tracked in these three cases are compared in Figures 7 and 8, and the control performance of the proposed adaptive backstepping controller in the first case is presented in Figures 9–14. In Figure 14, $e_{1i}, \varepsilon_{1i}, \xi_{1i}, i = 1, 2$, are

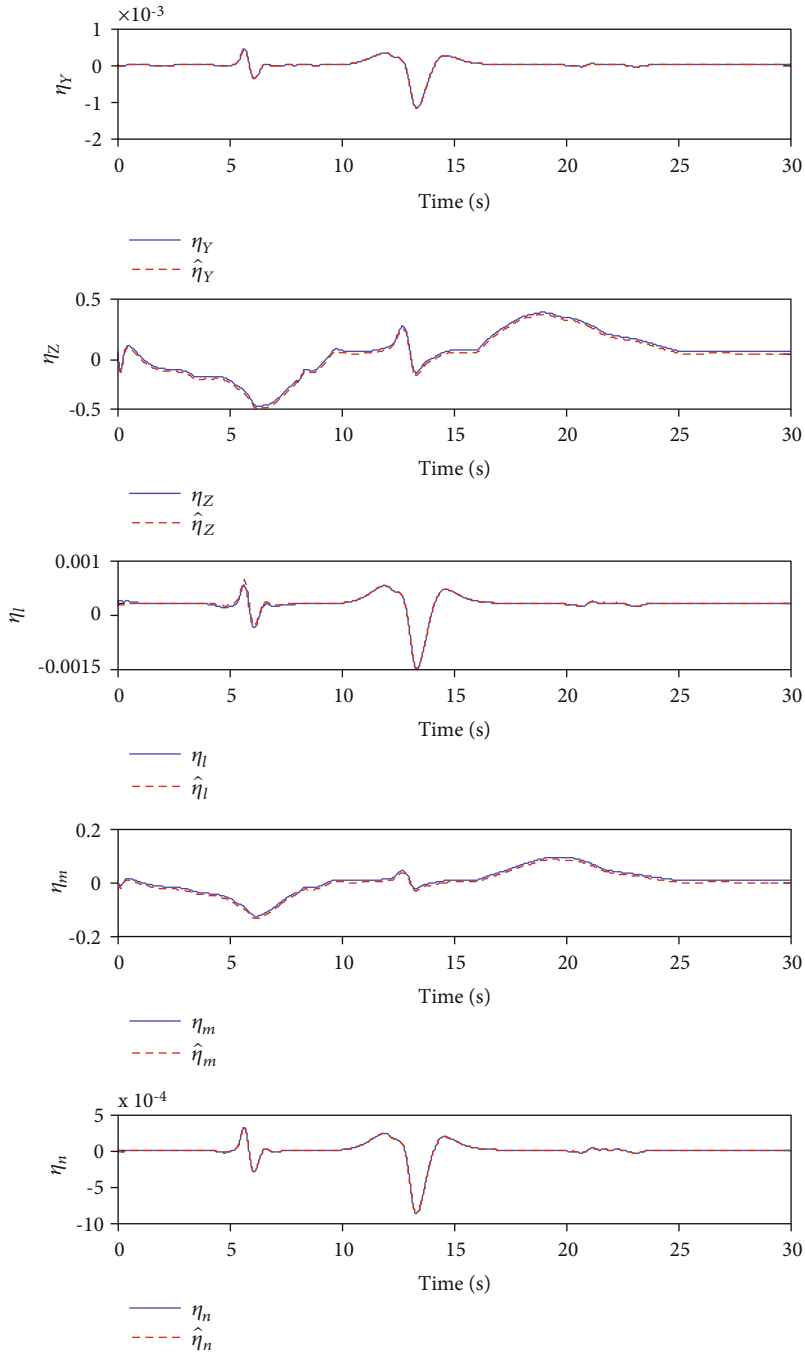

Figure 12: Observation of the unsteady aerodynamic states.

components of $e_1, \varepsilon_1, \xi_1$, respectively; $e_{2i}, \varepsilon_{2i}, \xi_{2i}$, $i = 1, 2, 3$ are components of $e_2, \varepsilon_2, \xi_2$, respectively. It can be observed from Figures 7 and 8 that the tracking performance of the first case outperforms the other two cases. It is apparent that smaller steady tracking errors and better transient tracking performances can be achieved since the effects of unsteady aerodynamics and uncertain parameters are both compensated. It also can be concluded that the unsteady aerodynamics seriously affects the aircraft dynamics and the compensation of unsteady effects could significantly improve the control performance. Note that the thrust force presented in Figure 9 increases drastically in the maneuver; it is quite rational for the pilot to increase the throttle to provide a larger thrust force when the fighter operates at high AOA. In addition, the aerodynamic surfaces are all set to zero when $\alpha > 55^\circ$ and the attitude control was completed via thrust vector merely in this deep stall area. From Figures 10–12, it can be seen that the tracking errors increase while the compensated errors still converge to zero even though thrust vector nozzles are saturated. Moreover, the proposed observer is effective in state reconstruction with strong robustness against parameter uncertainties, especially in the lateral channel. Meanwhile,

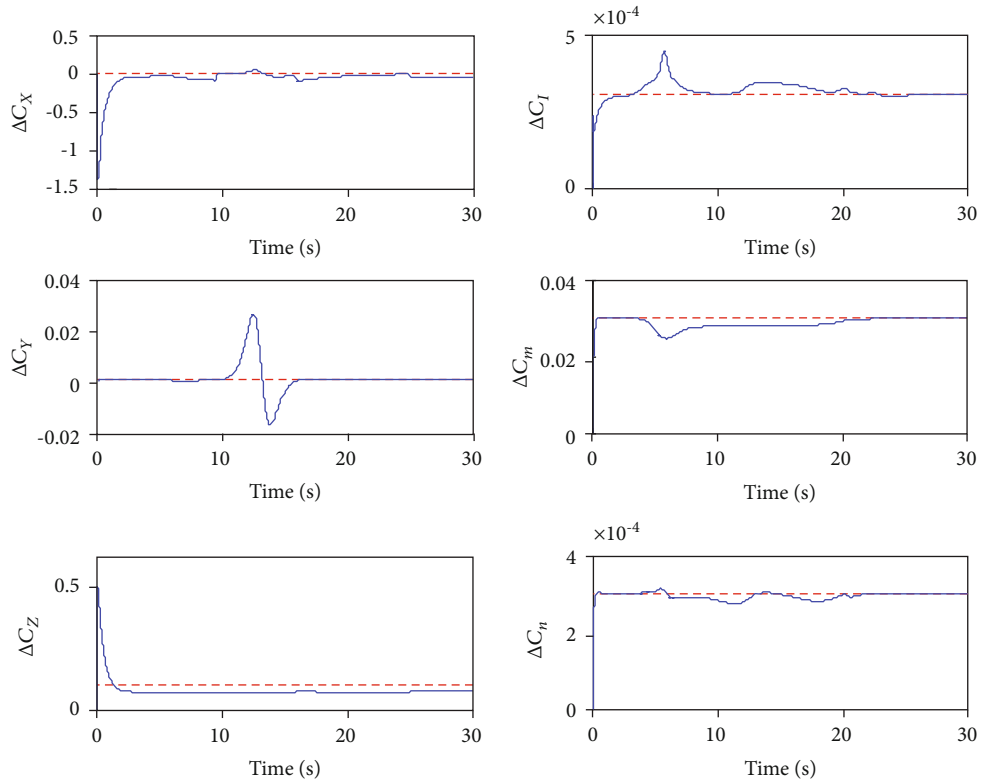

Figure 13: Estimation of the uncertain parameters.

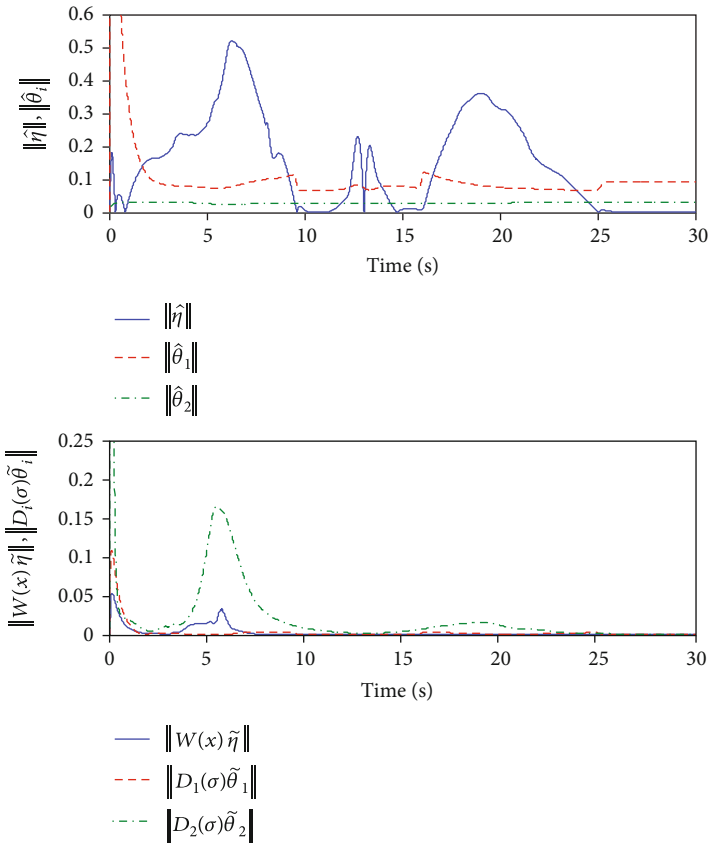

Figure 14: Time histories of the norms.

the parameter estimator works fairly well in the presence of unsteady effects. The most essential reason can be concluded that the converging rate of state reconstruction error is much larger than the estimate error, thus the mutual effects nearly can be ignored. Figure 13 shows the uncertain parameters in aerodynamic moments are estimated exactly, but steady errors exist in the estimation of aerodynamic force parameters. This is consistent with the discussion in previous subsection. However, as presented in Figure 14, $\mathbf{W}(\mathbf{x})\tilde{\eta}, \mathbf{D}_1(\sigma)\widetilde{\theta}_1$, and $\mathbf{D}_2(\sigma)\widetilde{\theta}_2$ all converge to zero after $t = 25.5$ s; the attractive manifold is achieved and the norms of the estimated states and parameters are maintained. Therefore, the performance of the deterministic control system is captured by the proposed constraint adaptive backstepping controller.

6. Conclusions

This paper is devoted to the constraint adaptive backstepping control design for the advanced fighter, where robust tracking of the predefined trajectories has been achieved. In particular, unsteady effects, parameter uncertainties, and input constraints are all considered which brings forward a great challenge for the control design. The proposed control scheme involves a state observer, a constraint backstepping controller, and two parameter estimators, which are designed separately. It should be pointed out that both the state observer and parameter estimator are designed based on the novel noncertainty equivalent principle which renders the closed-loop system with deterministic control performance. Moreover, stability of the closed-loop system can be guaranteed even though the saturation occurs. It can be concluded from simulation results that the backstepping controller integrated with the NCEA law outperforms the traditional adaptive backstepping controller. The effectiveness and robustness of the proposed control scheme are also verified by the Herbst maneuver. This paper mainly focuses on the theoretical aspect; our future work will be devoted to the practical applications of the flight control of scaled aircraft.

Appendix

The expressions of $\mathbf{f}_1(\mathbf{x}), \mathbf{f}_2(\mathbf{x}), \mathbf{W}_1(\mathbf{x}), \mathbf{W}_2(\mathbf{x}), \mathbf{D}_1(\sigma), \mathbf{D}_2(\sigma), \mathbf{G}_2(\sigma)$ are given as follows:

$$\mathbf{f}_1(\mathbf{x}) = \begin{bmatrix} f_\alpha \\ f_\beta \end{bmatrix} = \begin{bmatrix} -p_s \tan\beta + \dfrac{G_z - QS(\bar{C}_X \sin\alpha - \bar{C}_Z \cos\alpha)}{mV_t \cos\beta} \\ \dfrac{G_y - QS(\bar{C}_X \cos\alpha \sin\beta - \bar{C}_Y \cos\beta + \bar{C}_Z \sin\alpha \sin\beta)}{mV_t} \end{bmatrix},$$

$$\mathbf{f}_2(\mathbf{x}) = \begin{bmatrix} r_s(f_\alpha + q) + (c_1 r + c_2 p)q \cos\alpha + (c_8 p - c_2 r)q \sin\alpha \\ c_5 pr - c_6(p^2 - r^2) \\ -p_s(f_\alpha + q) - (c_1 r + c_2 p)q \sin\alpha + (c_8 p - c_2 r)q \cos\alpha \end{bmatrix} + \begin{bmatrix} QSb[\bar{C}_l(c_3 \cos\alpha + c_4 \sin\alpha) + \bar{C}_n(c_4 \cos\alpha + c_9 \sin\alpha)] \\ c_7 QS\bar{c}\bar{C}_m \\ -QSb[\bar{C}_l(c_3 \sin\alpha - c_4 \cos\alpha) + \bar{C}_n(c_4 \sin\alpha - c_9 \cos\alpha)] \end{bmatrix},$$

$$\mathbf{W}_1(\mathbf{x}) = \frac{QS}{mV_t} \begin{bmatrix} 0 & \dfrac{\cos\alpha}{\cos\beta} & 0 & 0 & 0 \\ \cos\beta & -\sin\alpha \sin\beta & 0 & 0 & 0 \end{bmatrix},$$

$$\mathbf{W}_2(\mathbf{x}) = QS \begin{bmatrix} 0 & \dfrac{r_s \cos\alpha}{mV_t \cos\beta} & b(c_3 \cos\alpha + c_4 \sin\alpha) & 0 & b(c_4 \cos\alpha + c_9 \sin\alpha) \\ 0 & 0 & 0 & c_7\bar{c} & 0 \\ 0 & \dfrac{-p_s \cos\alpha}{mV_t \cos\beta} & b(-c_3 \sin\alpha + c_4 \cos\alpha) & 0 & b(-c_4 \sin\alpha + c_9 \cos\alpha) \end{bmatrix},$$

$$\mathbf{D}_1(\sigma) = \frac{QS}{mV_t} \begin{bmatrix} -\dfrac{\sin\alpha}{\cos\beta} & 0 & \dfrac{\cos\alpha}{\cos\beta} \\ -\cos\alpha \sin\beta & \cos\beta & -\sin\alpha \sin\beta \end{bmatrix},$$

$$\mathbf{D}_2(\sigma) = QS \begin{bmatrix} b(c_3 \cos\alpha + c_4 \sin\alpha) & 0 & b(c_4 \cos\alpha + c_9 \sin\alpha) \\ 0 & c_7\bar{c} & 0 \\ b(-c_3 \sin\alpha + c_4 \cos\alpha) & 0 & b(-c_4 \sin\alpha + c_9 \cos\alpha) \end{bmatrix},$$

$$\mathbf{G}_2(\sigma) = \begin{bmatrix} g_{11} & 0 & g_{13} & g_{14} & g_{15} & g_{16} & g_{17} \\ 0 & g_{22} & 0 & 0 & 0 & g_{26} & g_{27} \\ g_{31} & 0 & g_{33} & g_{34} & g_{35} & g_{36} & g_{37} \end{bmatrix}, \quad \text{(A.1)}$$

$$g_{11} = QSb\left[\left(c_3 C_{l\delta_a} + c_4 C_{n\delta_a}\right) \cos\alpha + \left(c_4 C_{l\delta_a} + c_9 C_{n\delta_a}\right) \sin\alpha\right],$$

$$g_{13} = QSb\left[\left(c_3 C_{l\delta_r} + c_4 C_{n\delta_r}\right) \cos\alpha + \left(c_4 C_{l\delta_r} + c_9 C_{n\delta_r}\right) \sin\alpha\right],$$

$$g_{14} = -(c_4 \cos\alpha + c_9 \sin\alpha)Tx_T,\ g_{15} = -(c_4 \cos\alpha + c_9 \sin\alpha)Tx_T,$$

$$g_{16} = \frac{(c_3 \cos\alpha + c_4 \sin\alpha)Ty_T}{2},\ g_{17} = \frac{-(c_3 \cos\alpha + c_4 \sin\alpha)Ty_T}{2},$$

$$g_{22} = c_7 QS\bar{c}C_{m\delta_e},\quad g_{26} = -c_7 Tx_T,\quad g_{27} = -c_7 Tx_T,$$

$$g_{31} = -QSb\left[\left(c_3 C_{l\delta_a} + c_4 C_{n\delta_a}\right) \sin\alpha - \left(c_4 C_{l\delta_a} + c_9 C_{n\delta_a}\right) \cos\alpha\right],$$

$$g_{33} = -QSb\left[\left(c_3 C_{l\delta_r} + c_4 C_{n\delta_r}\right) \sin\alpha - \left(c_4 C_{l\delta_r} + c_9 C_{n\delta_r}\right) \cos\alpha\right],$$

$$g_{34} = (c_4 \sin\alpha - c_9 \cos\alpha)Tx_T,\ g_{35} = (c_4 \sin\alpha - c_9 \cos\alpha)Tx_T,$$

$$g_{36} = \frac{(-c_3 \sin\alpha + c_4 \cos\alpha)Ty_T}{2},\quad g_{37} = \frac{(c_3 \sin\alpha - c_4 \cos\alpha)Ty_T}{2}. \quad \text{(A.2)}$$

Nomenclature

m: Aircraft mass
V_t: Airspeed
$b, \bar{c}$: Wing span and mean aerodynamic chord
Q: Dynamic pressure
S: Reference area

I_{xz}: Product moment of inertia
T: Total thrust force
α, β: Angle of attack and sideslip angle
p, q, r: Body-axis roll, pitch, and yaw rates
p_s, q_s, r_s: Stability-axis roll, pitch, and yaw rates
$C_{Y\delta_a}, C_{Y\delta_r}, C_{Z\delta_e}, C_{l\delta_a}, C_{l\delta_r}, C_{m\delta_e}, C_{n\delta_a}, C_{n\delta_r}$: Control derivatives
I_x, I_y, I_z: Roll, pitch, and yaw moments of inertia
L_A, M_A, N_A: Aerodynamic moments along body axis system
L_T, M_T, N_T: Thrust moments along body axis system
G_x, G_y, G_z: Gravity components along body axis system
$\delta_a, \delta_e, \delta_r$: Aileron, elevator, and rudder deflections
δ_{yl}, δ_{zl}: Left nozzle deflections in yaw and pitch plane
δ_{yr}, δ_{zr}: Right nozzle deflections in yaw and pitch plane
x_T, z_T: Thrust point x-axis and z-axis locations
T_x, T_y, T_z: Thrust forces along body axis system
$\bar{X}, \bar{Y}, \bar{Z}$: Aerodynamic forces along body axis system.

Data Availability

The data used to support the findings of this study are included within the article.

Conflicts of Interest

The authors declare that they have no conflicts of interest.

Acknowledgments

This study was cosupported in part by the National Natural Science Foundation of China under Grants 61673240 and 61873278.

References

[1] M. Xin, "Unified nonlinear optimal flight control and state estimation of highly maneuverable aircraft," *Aerospace Science and Technology*, vol. 37, pp. 70–80, 2014.

[2] Y. Shin, A. J. Calise, and M. D. Johnson, "Adaptive control of advanced fighter aircraft in nonlinear flight regimes," *Journal of Guidance, Control, and Dynamics*, vol. 31, no. 5, pp. 1464–1477, 2008.

[3] S. Sieberling, Q. P. Chu, and J. A. Mulder, "Robust flight control using incremental nonlinear dynamic inversion and angular acceleration prediction," *Journal of Guidance, Control, and Dynamics*, vol. 33, no. 6, pp. 1732–1742, 2010.

[4] B. Erginer and E. Altug, "Design and implementation of a hybrid fuzzy logic controller for a quadrotor VTOL vehicle," *International Journal of Control, Automation and Systems*, vol. 10, no. 1, pp. 61–70, 2012.

[5] G. S. Lakshmikanth, R. Padhi, J. M. Watkins, and J. E. Steck, "Adaptive flight-control design using neural network aided optimal nonlinear dynamic inversion," *Journal of Aerospace Information Systems*, vol. 11, no. 11, pp. 785–806, 2014.

[6] M. R. Mokhtari and B. Cherki, "A new robust control for mini-rotorcraft unmanned aerial vehicles," *ISA Transactions*, vol. 56, pp. 86–101, 2015.

[7] S. Mondal and C. Mahanta, "Chattering free adaptive multivariable sliding mode controller for systems with matched and mismatched uncertainty," *ISA Transactions*, vol. 52, no. 3, pp. 335–341, 2013.

[8] Y. He, H. Pei, and T. Sun, "Robust tracking control of helicopters using backstepping with disturbance observers," *Asian Journal of Control*, vol. 16, no. 5, pp. 1387–1402, 2014.

[9] C. Peng, Y. Bai, X. Gong, Q. Gao, C. Zhao, and Y. Tian, "Modeling and robust backstepping sliding mode control with adaptive RBFNN for a novel coaxial eight-rotor UAV," *IEEE/-CAA Journal of Automatica Sinica*, vol. 2, no. 1, pp. 56–64, 2015.

[10] Z. Liu, X. Tan, R. Yuan, G. Fan, and J. Yi, "Adaptive trajectory tracking control system design for hypersonic vehicles with parametric uncertainty," *Proceedings of the Institution of Mechanical Engineers, Part G: Journal of Aerospace Engineering*, vol. 229, no. 1, pp. 119–134, 2015.

[11] J. Cayero, B. Morcego, and F. Nejjari, "Modelling and adaptive backstepping control for TX-1570 UAV path tracking," *Aerospace Science and Technology*, vol. 39, pp. 342–351, 2014.

[12] Y. Lv, Q. Hu, G. Ma, and J. Zhou, "6 DOF synchronized control for spacecraft formation flying with input constraint and parameter uncertainties," *ISA Transactions*, vol. 50, no. 4, pp. 573–580, 2011.

[13] N. O. Pérez-Arancibia, T. C. Tsao, and J. S. Gibson, "Saturation-induced instability and its avoidance in adaptive control of hard disk drives," *IEEE Transactions on Control Systems Technology*, vol. 18, no. 2, pp. 368–382, 2010.

[14] J. Farrell, M. Sharma, and M. Polycarpou, "Backstepping-based flight control with adaptive function approximation,"

Journal of Guidance, Control, and Dynamics, vol. 28, no. 6, pp. 1089–1102, 2005.

[15] M. Chen, S. S. Ge, and B. How, "Robust adaptive neural network control for a class of uncertain MIMO nonlinear systems with input nonlinearities," *IEEE Transactions on Neural Networks*, vol. 21, no. 5, pp. 796–812, 2010.

[16] M. Chen, S. S. Ge, and B. Ren, "Adaptive tracking control of uncertain MIMO nonlinear systems with input constraints," *Automatica*, vol. 47, no. 3, pp. 452–465, 2011.

[17] Q. Zong, F. Wang, and B. L. Tian, "Nonlinear adaptive filter backstepping flight control for reentry vehicle with input constraint and external disturbances," *Proceedings of the Institution of Mechanical Engineers, Part G: Journal of Aerospace Engineering*, vol. 228, no. 6, pp. 889–907, 2014.

[18] Q. Zong, F. Wang, B. Tian, and R. Su, "Robust adaptive approximate backstepping control of a flexible air-breathing hypersonic vehicle with input constraint and uncertainty," *Proceedings of the Institution of Mechanical Engineers, Part I: Journal of Systems and Control Engineering*, vol. 228, no. 7, pp. 521–539, 2014.

[19] X. Bu, X. Wu, M. Tian, J. Huang, R. Zhang, and Z. Ma, "High-order tracking differentiator based adaptive neural control of a flexible air-breathing hypersonic vehicle subject to actuators constraints," *ISA Transactions*, vol. 58, pp. 237–247, 2015.

[20] W. Dong, J. A. Farrell, M. M. Polycarpou, V. Djapic, and M. Sharma, "Command filtered adaptive backstepping," *IEEE Transactions on Control Systems Technology*, vol. 20, no. 3, pp. 566–580, 2012.

[21] L. Sonneveldt, Q. P. Chu, and J. A. Mulder, "Nonlinear flight control design using constrained adaptive backstepping," *Journal of Guidance, Control, and Dynamics*, vol. 30, no. 2, pp. 322–336, 2007.

[22] J. Zhu, S. Zhang, and C. Zhou, "Dynamic characteristics and challenges for control system of super-maneuverable aircraft," *Journal of Control Theory and Applications*, vol. 31, no. 12, pp. 1650–1662, 2014.

[23] A. Astolfi and R. Ortega, "Immersion and invariance: a new tool for stabilization and adaptive control of nonlinear systems," *IEEE Transactions on Automatic Control*, vol. 48, no. 4, pp. 590–606, 2003.

[24] A. Astolfi, D. Karagiannis, and R. Ortega, *Nonlinear and Adaptive Control with Applications*, Springer, London, UK, 2008.

[25] D. Karagiannis and A. Astolfi, "Nonlinear and adaptive flight control of autonomous aircraft using invariant manifolds," *Proceedings of the Institution of Mechanical Engineers, Part G*, vol. 224, no. 4, pp. 403–415, 2009.

[26] K. W. Lee and S. N. Singh, "Immersion- and invariance-based adaptive missile control using filtered signals," *Proceedings of the Institution of Mechanical Engineers, Part G: Journal of Aerospace Engineering*, vol. 226, no. 6, pp. 646–663, 2012.

[27] J. Zhang, Q. Li, N. Cheng, and B. Liang, "Adaptive dynamic surface control for unmanned aerial vehicles based on attractive manifolds," *Journal of Guidance, Control, and Dynamics*, vol. 36, no. 6, pp. 1776–1783, 2013.

[28] D. Karagiannis, M. Sassano, and A. Astolfi, "Dynamic scaling and observer design with application to adaptive control," *Automatica*, vol. 45, no. 12, pp. 2883–2889, 2009.

[29] D. Seo and M. R. Akella, "High-performance spacecraft adaptive attitude-tracking control through attracting-manifold design," *Journal of Guidance, Control, and Dynamics*, vol. 31, no. 4, pp. 884–891, 2008.

[30] D. Seo and M. R. Akella, "Non-certainty equivalent adaptive control for robot manipulator systems," *Systems and Control Letters*, vol. 58, no. 4, pp. 304–308, 2009.

[31] B. Zhao, B. Xian, Y. Zhang, and X. Zhang, "Nonlinear robust adaptive tracking control of a quadrotor UAV via immersion and invariance methodology," *IEEE Transactions on Industrial Electronics*, vol. 62, no. 5, pp. 2891–2902, 2015.

[32] D. Seo, "Fast adaptive pose tracking control for satellites via dual quaternion upon non-certainty equivalence principle," *Acta Astronautica*, vol. 115, pp. 32–39, 2015.

[33] A. Mannarino and P. Mantegazza, "Multifidelity control of aeroelastic systems: an immersion and invariance approach," *Journal of Guidance, Control, and Dynamics*, vol. 37, no. 5, pp. 1568–1582, 2014.

[34] A. Astolfi, R. Ortega, and A. Venkatraman, "A globally exponentially convergent immersion and invariance speed observer for mechanical systems with non-holonomic constraints," *Automatica*, vol. 46, no. 1, pp. 182–189, 2010.

[35] C. Zhou, J. Zhu, H. Lei, X. Yuan, and W. Wang, "Robust constraint backstepping control for high-performance aircraft with account of unsteady aerodynamic effects," *Proceedings of the Institution of Mechanical Engineers, Part G: Journal of Aerospace Engineering*, vol. 230, no. 13, pp. 2484–2503, 2016.

[36] C. Zhou, J. Zhu, H. Lei, and X. Yuan, "Observer-based dynamic surface control for high-performance aircraft subjected to unsteady aerodynamics and actuator saturation," *Proceedings of the Institution of Mechanical Engineers, Part I: Journal of Systems and Control Engineering*, vol. 231, no. 6, pp. 481–494, 2017.

[37] Q. Wang, K.-F. He, W.-Q. Qian, T.-J. Zhang, Y.-Q. Cheng, and K.-Y. Wu, "Unsteady aerodynamics modeling for flight dynamics application," *Acta Mechanica Sinica*, vol. 28, no. 1, pp. 14–23, 2012.

[38] S. L. Brunton, S. T. M. Dawson, and C. W. Rowley, "State-space model identification and feedback control of unsteady aerodynamic forces," *Journal of Fluids and Structures*, vol. 50, pp. 253–270, 2014.

[39] J. Hu and H. Zhang, "Immersion and invariance based command-filtered adaptive backstepping control of VTOL vehicles," *Automatica*, vol. 49, no. 7, pp. 2160–2167, 2013.